

# Optimization of low-carbon multi-energy systems with seasonal geothermal energy storage: The Energy Grid of ETH Zurich

**Journal Article****Author(s):**

Gabrielli, Paolo ; Acquilino, Alberto; Siri, Silvia; Bracco, Stefano; Sansavini, Giovanni; Mazzotti, Marco

**Publication date:**

2020-12

**Permanent link:**

<https://doi.org/10.3929/ethz-b-000440520>

**Rights / license:**

[Creative Commons Attribution 4.0 International](#)

**Originally published in:**

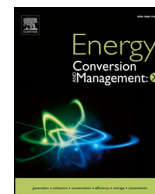
Energy Conversion and Management 8, <https://doi.org/10.1016/j.ecmx.2020.100052>



ELSEVIER

Contents lists available at ScienceDirect

## Energy Conversion and Management: X

journal homepage: [www.journals.elsevier.com/energy-conversion-and-management-x](http://www.journals.elsevier.com/energy-conversion-and-management-x)

# Optimization of low-carbon multi-energy systems with seasonal geothermal energy storage: The Anergy Grid of ETH Zurich

Paolo Gabrielli<sup>a</sup>, Alberto Acquilino<sup>a</sup>, Silvia Siri<sup>b</sup>, Stefano Bracco<sup>c</sup>, Giovanni Sansavini<sup>a</sup>, Marco Mazzotti<sup>d,\*</sup>

<sup>a</sup> Institute of Energy and Process Engineering, Reliability and Risk Engineering, ETH Zurich, 8092 Zurich, Switzerland

<sup>b</sup> Department of Informatics, Bioengineering, Robotics and Systems Engineering, University of Genoa, 16145 Genoa, Italy

<sup>c</sup> Electrical, Electronics and Telecommunication Engineering and Naval Architecture Department (DITEN), University of Genoa, 16145 Genoa, Italy

<sup>d</sup> Institute of Energy and Process Engineering, Separation Processes Laboratory, ETH Zurich, 8092 Zurich, Switzerland

## ARTICLE INFO

## Keywords:

Multi-energy systems  
Seasonal storage  
Geothermal storage  
Energy networks  
MINLP  
Yearly scheduling

## ABSTRACT

We investigate the optimal operation of multi-energy systems deploying geothermal energy storage to deal with the seasonal variability of heating and cooling demands. We do this by developing an optimization model that improves on the state-of-the-art by accounting for the nonlinearities of the physical system, and by capturing both the short- and long-term dynamics of energy conversion, storage and consumption. The algorithm aims at minimizing the CO<sub>2</sub> emissions of the system while satisfying the heating and cooling demands of given end-users, and it determines the optimal operation of the system, i.e. the mass flow rate and temperature of the water circulating through the network, accounting for the time evolution of the temperature of the geothermal fields.

This optimization model is developed with reference to a real-world application, namely the *Anergy Grid* installed at ETH Zurich, in Switzerland. Here, centralized heating and cooling provision based on fossil fuels is complemented by a dynamic underground network connecting geothermal fields, acting as energy source and storage, and demand end-users requiring heating and cooling energy. The proposed optimization algorithm allows reducing the CO<sub>2</sub> emissions of the university campus by up to 87% with respect to the use of a conventional system based on centralized heating and cooling. This improves on the 72% emissions reduction achieved with the current operation strategies. Furthermore, the analysis of the system allows to derive design guidelines and to explain the rationale behind the operation of the system. The study highlights the importance of coupling daily and seasonal energy storage towards the achievement of low-carbon energy systems.

## 1. Introduction

The evidence of climate change clearly indicates the necessity of new routes for energy supply, entailing zero-carbon emissions around 2050 and limiting global warming at 1.5 °C [1]. New routes of energy provision are enabled by distributed generation, smart grids and smart energy networks concepts, all seen as a viable solution to reduce primary energy use and carbon dioxide (CO<sub>2</sub>) emissions, as well as to increase the reliability and the flexibility of electrical and thermal networks [2–6].

In this context, multi-energy systems (MES) represent a new paradigm that exploits the interaction among various energy carriers, such as heat and cold, both at design and operation phase, allowing for improved technical, economic and environmental performance of the integrated energy system [7–9]. MES can provide energy to a single dwelling, a group of buildings, a single firm, a district or a region. The coupling of

multiple energy vectors determines a greater complexity of urban energy systems [10]. Reference [7] provides a detailed overview of MES, focusing on the identification of internal and external energy flows, and proposes criteria for their technical and economic evaluation.

The spread of MES transforms energy end-users into prosumers, which are both self-consumers and providers of the energy supply [11]. Local energy communities arise to optimally operate such MES facilities from both technical, economic and environmental standpoints [12,13]. Such communities are usually composed of several energy hubs, each characterized by specific electrical, thermal and cooling energy needs. Particularly in the tertiary and residential sectors, often characterized by a significant degree of electrification, heat pumps constitute an efficient technology to provide heat and cooling energy by exploiting different primary sources, i.e. air, water and ground [14–16]. The flexibility of heat pumps can be exploited to provide ancillary services

\* Corresponding author.

E-mail address: [marco.mazzotti@ipe.mavt.ethz.ch](mailto:marco.mazzotti@ipe.mavt.ethz.ch) (M. Mazzotti).

<https://doi.org/10.1016/j.ecmx.2020.100052>

Nomenclature		Sets	
<i>Symbols</i>		$\mathcal{B}$	set of branches of thermal network
$A$	heat exchange area, [m <sup>2</sup> ]	$\mathcal{C}$	set of energy carriers
$c$	specific heat of water, [kJ/(kg K)]	$\mathcal{D}$	set of clusters
$D$	carrier demand, [kWh]	$\mathcal{G}$	set of geothermal fields
$d$	binary defining flow direction in network branches	$\mathcal{I}$	set of intersection points of thermal network
$E$	energy stored in hot water thermal storage, [kWh]	$\mathcal{M}$	set of available technologies
$e$	CO <sub>2</sub> emissions, [gCO <sub>2</sub> ]	$\mathcal{MD}$	set of technologies available in the clusters
$F$	input power, [kW]	$\mathcal{O}$	set of all nodes of thermal network
$g$	function defining dynamic behavior of geothermal fields	<i>Subscripts</i>	
$H$	number of yearly operating hours	HT	high temperature
$h$	function defining thermal losses of hot water thermal storage	LT	low temperature
$L$	depth of geothermal fields, [m]	<i>Superscripts</i>	
$m$	mass flow rate, [kg/s]	amb	ambient
$\tilde{m}$	auxiliary variable for MILP relaxation [kg K/s]	b	borehole
$n$	number of boreholes	c	cooling
$P$	output power, [kW]	cond	condensation
$Q$	net injected thermal power, [kW]	eva	evaporation
$R$	thermal resistance, [m K/W]	F	geothermal field
$r$	radius of the geothermal field, [m]	in	inlet
$S$	technology size, [kW]	int	internal
$s$	number of yearly switches	max	maximum
$T$	temperature, [K]	min	minimum
$U$	overall heat transfer coefficient, [W/K m <sup>2</sup> ]	out	outlet
$u$	import energy price, [EUR/kWh]	w	wall
$v$	export energy price, [EUR/kWh]	<i>Acronyms</i>	
$x$	binary defining scheduling of cluster technology	AG	Anergy Grid
$y$	binary defining node configuration	B	Boiler
<i>Greek symbols</i>		C	Compression Chiller
$\alpha$	thermal diffusivity of soil, [m <sup>2</sup> /s]	EMS	Energy Management Systems
$\beta$	parameter defining temperature dependence of technology performance	GF	Geothermal Field
$\gamma$	Euler-Mascheroni constant	HE	Heat Exchanger
$\delta$	parameter defining minimum size constraint	HP	Heat Pump
$\epsilon$	carrier carbon intensity, [gCO <sub>2</sub> /kWh]	HT	High-Temperature
$\zeta$	mass flow rate multiplication factor	HTHE	High-Temperature Heat Exchanger
$\eta$	technology efficiency	LT	Low-Temperature
$\kappa$	mass flow rate additive factor	LTHE	Low-Temperature Heat Exchanger
$\Lambda$	self-discharge efficiency, [1/h]	MES	Multi-Energy Systems
$\lambda$	thermal conductivity of soil, [W/(K m)]	MILP	Mixed-Integer Linear Program
$\mu$	normalized average mass flow rate	MINLP	Mixed-Integer NonLinear Program
$\nu$	mass flow rate constant factor	HWTS	Hot Water Thermal Storage
$\xi$	Carnot efficiency	PV	Photo-Voltaic
$\Pi$	ambient thermal losses		
$\tau$	charging/discharging time, [1/h]		
$\phi$	normalized energy dissipated to the environment		

to the electric power system by load modulation strategies [17], and geothermal distributed heat pumps can be operated to provide heat peak demand shaving within a district heating network [18].

Several local, district and city-scale MES are coupled to geothermal sources in urban ground and groundwater [19–21]. In these cases, the optimal design of geothermal heat pumps and borehole heat exchangers is challenging; different local factors have to be examined, such as the available space, the geomorphology of the site and the ground thermal response [22,23,21]. As far as the geothermal field is concerned, open- or closed-loop systems having a vertical or horizontal arrangement of boreholes, U-tube or spiral shaped, have to be examined very carefully since errors during the design phase can lead to malfunctioning of the whole

geothermal system. Innovative solutions consider ground source heat pump systems coupled with PV and solar thermal collectors to reduce the land use [24,25], or geothermal combined heat and power plants [26–28].

The deployment of MES is often coupled with energy storage technologies, which allow to compensate fluctuations in renewable energy production and energy demand [29–31]. Concerning thermal storage, two categories of systems are used to compensate short-term and long-term fluctuations. Daily or weekly fluctuations can be compensated by water tank storages, referred to as hot water thermal storage (HWTS), whereas long-term fluctuations can be compensated via phase change materials and geothermal installations [32,33,15]. However, compensating variable energy generation and demand at the seasonal scale is daunting, because (i) it can

only be done through a few, expensive technologies, such as underground geothermal installations, and (ii) the optimal design and operation is complicated by the large number of decision variables, due to the required length and resolution of the time horizon [29,34,35], and by the system complexity.

Several tools for energy management systems (EMS) are proposed in the literature to optimally design and operate MES systems with energy storage [10,36]. EMS can be based on linear or non-linear mathematical models, can be characterized by single- or multi-objective optimization frameworks and capture the physics of the elements of the energy system with different levels of detail [37,10]. Concerning the optimal design and operation of seasonal storage systems, some studies have recently tackled the complexity of the optimization problem by using time series aggregation methods, i.e. by reducing the number of time intervals while retaining a level of detail sufficient to describe the dynamics of the entire energy system. A review of these methods is provided by Hoffmann et al. [35], Schütz et al. [38], and Gabrielli [39].

Modeling seasonal storage offers the opportunity to assess strategies for offsetting the seasonal variability of heating and cooling demands [40]. A real-world system adopting this concept is the Anergy Grid installed at ETH Zurich, in Switzerland, which consists of an underground network deploying geothermal fields acting as energy sources and storage units [41]. The current system operation allows reducing the CO<sub>2</sub> emissions of the university campus by 72% with respect to the conventional system using centralized heating and cooling [42]. The scope of this contribution is to develop an optimization framework enabling further increase in energy efficiency, hence further emissions reduction.

The full potential of the system can only be exploited by adopting an optimization-based EMS able to (i) describe the underground network structure, (ii) capture the short- and long-term dynamics of energy production, storage and consumption, (iii) account for the different temperature levels at which heat and cold are required during the year, (iv) model the time evolution of the geothermal fields, (v) model the scheduling of the conversion technologies installed in the demand clusters. Whereas previous studies have investigated the optimal design and operation of MES coupled with geothermal systems [43–45], and the optimal design and operation of MES coupled with heating networks [46–48], two important aspects remain uncovered. On the one hand, such studies do not consider the different temperature levels at which heat and cold demands are required.

Although this assumption is reasonable for systems where heat and cold are provided by separate units, and allows preserving the linearity of the optimization problem with the associated computational complexity, it prevents the analysis of systems where heat and cold are provided through the same network. On the other hand, the system behavior is investigated during a few representative days along the year, but the interaction between daily and seasonal system dynamics is not accounted for.

These shortcomings stem from the computational complexity arising when describing the non-linear behavior of the system across different time scales. We tackle them by formulating a mixed-integer nonlinear program (MINLP) that accurately describes the physical behavior of the system, and by reducing it to a mixed-integer linear program (MILP) that is able to capture the most relevant aspects and features a reasonable computational complexity. This optimization algorithm aims at minimizing the CO<sub>2</sub> emissions of the multi-energy system while satisfying the heating and cooling demands of end-users. It determines the optimal operation of the system, i.e. the mass flow rate and temperature of the water circulating through the network, and the resulting time evolution of the temperature of the geothermal fields. The optimal solution requires the knowledge of the energy demands, the energy prices, the carbon intensities of the energy grids, and the parameters characterizing the technical performance of the technologies involved. The developed optimization model builds on previously presented work [29,49,50] and introduces novel elements by: (i) developing detailed first-principle models and corresponding linear reduced order models to describe the geothermal fields, acting as seasonal storage devices; (ii) formulating and solving a MINLP optimization problem able to determine the optimal value of both the mass flow rate and the temperature of the water circulating in the network; (iii) modeling the structure of the geothermal network; (iv) determining optimal strategies to reduce the carbon footprint of the system and assessing potential savings with respect to currently adopted strategies.

Several techniques have been proposed to solve MINLP. As an example, Elsidio et al. presented bilevel decomposition algorithms able to determine the most profitable synthesis and design of combined heat and power units within a district heating network with thermal storage, while taking into account the yearly scheduling of the system [51,52]. Inspired by their work, we present a two-stage algorithm, where the

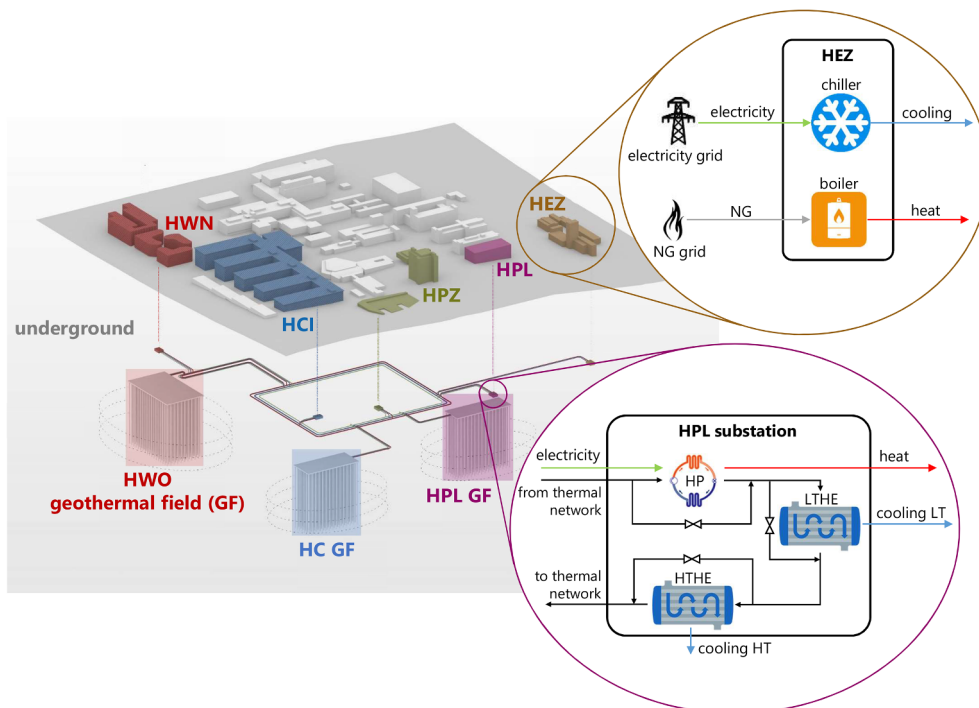


Fig. 1. Schematic of the Anergy Grid (AG) system installed at ETH Zurich, adapted from [41].

original MINLP is linearized by means of McCormick envelopes [53] and the resulting MILP is used to (i) determine a lower bound of the original optimization problem, and (ii) derive information on the optimal time profile of the mass flow rate.

The paper is structured as follows. Section 2 describes the investigated system. Section 3 presents the MINLP optimization problem, while Section 4 presents the linearization and solution techniques. Section 5 discusses the optimization results for the Anergy Grid of ETH Zurich. Finally, in Section 6 conclusions are drawn.

## 2. System description

The Anergy Grid of ETH Zurich is illustrated in Fig. 1; it consists of various underground geothermal fields, which are connected to the served demand clusters, i.e. clusters of buildings of the campus, through a low-temperature water network. More specifically, the system consists of five demand clusters, namely HPL, HPZ, HWN, HCP, HCO (last two included in HCI in Fig. 1), three geothermal fields, namely HPL, HC, HWO, and the centralized heat and cold generation plant, HEZ. The heat and cold generated by HEZ are directly supplied to the five demand clusters using a dedicated connection to each demand cluster, without transiting to the Anergy Grid. The geothermal fields consist of 200 m deep vertical U-shaped borehole heat exchangers. They are used as the energy source, as well as seasonal storage systems to exploit the seasonal shift between heat and cold demands. Each demand cluster includes a substation, which couples the demand cluster and the thermal network as detailed in Fig. 1 with reference to the HPL substation located in the HPL demand cluster. In the five substations, the heat and cold delivered to the buildings are actually produced. Heat is produced via heat pumps (HP) that transfer energy from the

underground water to a working fluid by absorbing electricity; cold is produced via two heat exchangers (HE): a low-temperature heat exchanger (LTHE) supplying the cooling demand of the laboratories, and a high-temperature heat exchanger (HTHE) supplying the cooling demand of air conditioning. If a substation requires heat, it is supplied from one of the other clusters or underground storages via the grid. If there is waste heat in a cluster, which cannot be directly used, it is either used by other clusters or stored in the underground storage, where it stays available for later use. The same applies to cold. The water network consists of two rings, one warm and one cold, with the temperatures varying between 8 °C and 22 °C.

The flexibility provided by the aforementioned design allows reducing the use of fossil-based technologies by exploiting the seasonal storage capacity of the geothermal fields. This is best achieved by keeping the temperature level of the storage low at the end of spring (i.e. at the end of the heating period), and high at the end of summer (i.e. at the end of the cooling period), so as to maximize the cooling and heating capacity in summer and winter, respectively [41]. During summer, the cooling demand of the clusters is high, and the water going from the substations to the geothermal fields is warmer than the soil. Hence, by circulating in the probes the water is cooled while heating up the ground; in this way, the water can absorb heat in the heat exchangers of the substation and provide cold. Such a process is reversed in winter: heat demand is high, the water going to the probes is colder than the ground and it is heated up while cooling down the ground, so as to provide heat to the clusters through the heat pumps of the substations. Whenever the Anergy Grid is not able to satisfy the energy demands, these are covered by using the conventional centralized boiler and the compression chiller unit.

Based on the continuous monitoring of the overall system, the first operating years have been evaluated. In 2016, the coverage of energy

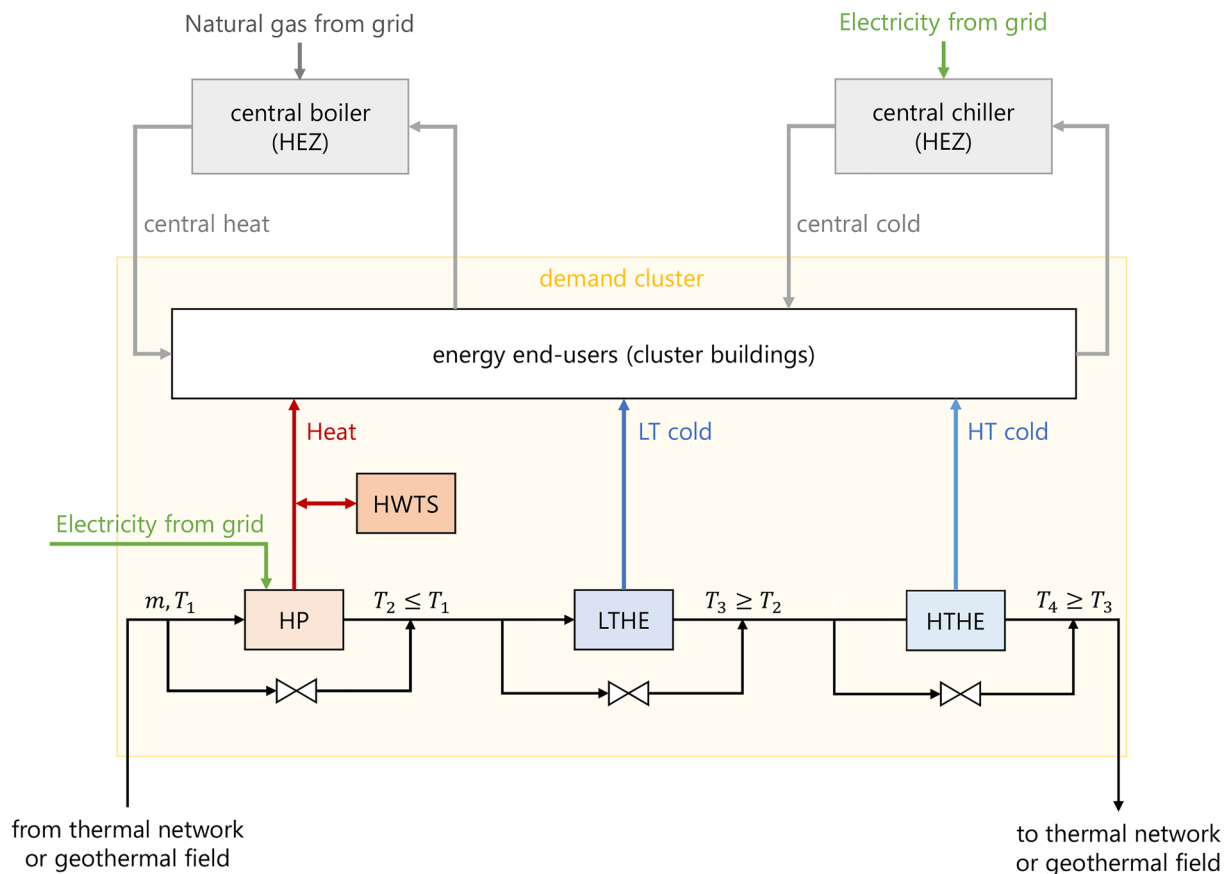


Fig. 2. Scheme of a single demand cluster. The yellow box contains the conversion substation and the energy end-users (cluster buildings). The substation consists of a heat pump (HP), a low-temperature heat exchanger (LTHE) and a high-temperature heat exchanger (HTHE) providing heat, LT cold and HT cold, respectively. When needed, heat and cold can be provided by the central system (HEZ). (For interpretation of the references to colour in this figure legend, the reader is referred to the web version of this article.)

requirements using the Anergy Grid was around 85% for the useful heating demand and 60% for the useful cold demand. The remaining amount was conventionally covered by using the centralized boiler and compression chiller unit [42].

In order to develop a general methodology for optimizing and assessing seasonal energy storage via geothermal networks, we model the Anergy Grid as a MES where several geothermal fields are used as energy source and storage, and are connected with several demand clusters through a low-temperature water network. The scheme of a demand clusters is illustrated in Fig. 2. The yellow box contains the cluster substation mentioned above and the energy end-users (buildings). In the substation, heat and cold are provided through the heat pump and the heat exchangers, respectively, by using the energy of the thermal network. When the thermal network cannot meet the energy demands, heat and cold are provided by the central boiler and the central compression chiller. The input and output energy flows defining such technologies, as well as the network temperatures, are function of time and are characterized for every time interval of the time horizon (one year with hour resolution here). Note that while one heat pump and two heat exchangers are installed for each cluster of the Anergy Grid, multiple heat pumps and heat exchangers could be used to provide heat and cold at different temperature levels.

The water coming from the network enters at temperature  $T_1$ . During the heating season, it goes through the heat pump and reduces its temperature to  $T_2$ ; the heat pump uses this low-temperature heat and electricity (from renewable energy sources) to provide high-temperature heat to the buildings. During the cooling season, the water coming from the network goes through the heat exchangers and increases its temperature to  $T_3$  (LTHE) and  $T_4$  (HTHE); the heat exchangers use this water to provide cold to the buildings. The heat pump and the heat exchanger can be operated separately (e.g. during peak heating or cooling seasons) or in combination (e.g., during mid seasons). They can even be operated in a closed loop, where the heat pump provides water at lower temperature to the heat exchanger, and the heat exchanger provides water at higher temperature to the heat pump.

The possibility of installing HWTS within the cluster substations is also considered. Due to the relatively high thermal losses, low thermal inertia and the low energy density, the HWTS is mostly used to offset short-term mismatch between energy production and demand.

### 3. System model and optimization framework

The optimal operation of the system described in Section 2 is identified through an optimization problem that minimizes the CO<sub>2</sub> emissions of the MES by determining the optimal flow rate and temperature of the water circulating in the geothermal network, as well as the optimal scheduling of heat pumps and heat exchangers, to satisfy the heating and cooling demands of the end-users. The resulting optimization tool must account for the different temperatures at which energy is required during the year, and therefore it is formulated as a MINLP. This can be written in general form as

$$\begin{aligned} & \min_{\mathbf{x}, \mathbf{y}} (\mathbf{c}_1^T \mathbf{x} + \mathbf{c}_2^T \mathbf{y}) \\ & \text{s. t.} \\ & f(\mathbf{x}, \mathbf{y}) = \mathbf{b} \\ & \mathbf{x} \geq \mathbf{0} \in \mathbb{R}^X, \quad \mathbf{y} \in \{0, 1\}^Y \end{aligned} \quad (1)$$

where  $\mathbf{c}_1$  and  $\mathbf{c}_2$  represent the cost vectors associated to the continuous and binary decision variables,  $\mathbf{x}$  and  $\mathbf{y}$ , respectively;  $f$  is a generic nonlinear function of  $\mathbf{x}$  and  $\mathbf{y}$ , where the nonlinearity arises due to the energy balances describing the thermal network and the technology behaviors, and  $\mathbf{b}$  is a constant vector;  $X$  and  $Y$  indicate the dimension of  $\mathbf{x}$  and  $\mathbf{y}$ , respectively. The binary variables model the non-linearities related to the scheduling (i.e. ON/OFF) of the conversion technologies and the direction of the water circulating in the thermal network.

The complexity of the considered MES requires an optimization tool able to capture both the short- and long-term dynamics of the energy

production, storage and consumption. Therefore, we consider a time horizon of one year with hourly resolution. Time series aggregation (method *M1* in reference [29]) is adopted to model the time horizon, thus reducing the computational burden resulting from the large number of decision variables, which is due to the complexity of the network and to the length and granularity of the time horizon. In the following, all the aspects of the optimization problem, namely input data, decision variables, constraints, and objective function are described in detail.

In the following, the set of energy carriers is indicated with  $\mathcal{C}$ , the set of clusters with  $\mathcal{D}$ , the set of geothermal fields with  $\mathcal{G}$ , and the set of intersection points of the thermal network with  $\mathcal{I}$ . The set of all nodes of the thermal network is denoted as  $\mathcal{O}$  and is the union of  $\mathcal{D}$ ,  $\mathcal{G}$  and  $\mathcal{I}$ . The set of branches departing from each node of the thermal network is denoted as  $\mathcal{B}$ . The set of available technologies is indicated with  $\mathcal{M}$ , whereas the set of technologies available in the clusters (i.e. heat pumps and heat exchangers) is indicated with  $\mathcal{M}_D$ . Unless otherwise indicated, bold symbols indicate vectors in  $\mathbb{R}^N$ , where  $N$  is the length of the time horizon.

#### 3.1. Input data

The carriers considered within the optimization problem are:

- Electricity (e). It can be imported from the electricity grid and is consumed by the heat pumps and by the conventional chiller unit.
- Natural gas (g). It can be imported from the natural gas distribution grid and is consumed by the conventional boiler.
- Heat (h). It is generated by the heat pumps and by the conventional boiler and is required by the clusters.
- Cold (c). It is generated by the heat exchangers and by the conventional chiller unit and is required by the clusters. Here, cold is required at two different levels, denoted as low-temperature (LT) and high-temperature (HT) cold (note that any number of cold levels could be considered).

Hourly-resolved profiles of 2018 are considered for the carrier demands (see Fig. S1 in the Appendix A). Inputs to the optimization problem are:

- Ambient temperature  $T^{\text{amb}}$
- Carrier demands  $D_{i,j}$   $\forall i \in \mathcal{D}, \forall j \in \mathcal{C}$
- Import and export carrier prices  $u_j, v_j$   $\forall j \in \mathcal{C}$
- Carrier carbon intensity  $\epsilon_j$   $\forall j \in \mathcal{C}$
- Technology size  $S_{i,k}$   $\forall i \in \mathcal{O}, \forall k \in \mathcal{M}$
- Parameters describing the technology performance (see Table 1).

#### 3.2. Decision variables

The following decision variables are returned by the optimization problem:

- Scheduling of cluster technologies  $\mathbf{x}_{i,k} \in \{0, 1\}^N$   $\forall i \in \mathcal{D}, \forall k \in \mathcal{M}_D$
- Water mass flow rate in the network nodes and branches  $\mathbf{m}_{i,l}$   $\forall i \in \mathcal{O}, \forall l \in \mathcal{B}$
- Inlet and outlet water temperature of clusters  $T_{i,k}^{\text{in}}, T_{i,k}^{\text{out}}$   $\forall i \in \mathcal{D}, \forall k \in \mathcal{M}_D$
- Inlet and outlet water temperature of geothermal fields  $T_j^{\text{in}}, T_j^{\text{out}}$   $\forall j \in \mathcal{G}$
- Average temperature of geothermal fields  $T_j^F$   $\forall j \in \mathcal{G}$
- Average water temperature in the network branches  $T_l$   $\forall l \in \mathcal{B}$
- Input power for all technologies and carriers  $F_{i,k,j}$   $\forall i \in \mathcal{D}, \forall k \in \mathcal{M}, \forall j \in \mathcal{C}$
- Output power for all technologies and carriers  $P_{i,k,j}$   $\forall i \in \mathcal{D}, \forall k \in \mathcal{M}, \forall j \in \mathcal{C}$
- Energy stored in hot water thermal storage  $E_i$   $\forall i \in \mathcal{D}$
- Flow direction in the network branches  $\mathbf{d}_l \in \{0, 1\}$   $\forall l \in \mathcal{B}$



### 3.3. Constraints

The constraints of the optimization problem can be grouped into two categories, namely the constraints representing the performance of conversion and storage technologies and the energy balances of the thermal network.

(I) **Performance of conversion and storage technologies.** The constraints reported in the following hold for all time intervals  $t \in \{1, \dots, N\}$  and the parameters describing the performance of the available technologies are reported in Table 1. The index specifying the energy carrier relative to the input and output powers is described in the text and is not reported in the equations for the sake of simplicity.

• *Conventional boiler and chiller.* For the boiler,  $P_t$  and  $F_t$  refer to generated thermal power and consumed fuel power (natural gas LHV), respectively. For the chiller,  $P_t$  and  $F_t$  refer to generated cooling power and consumed electrical power, respectively. For both technologies, the generated power is

$$P_t = \eta F_t \quad (2)$$

where

$$0 \leq F_t \leq S \quad (3)$$

Here,  $\eta$  is a constant conversion efficiency and  $S$  the size of the technology, i.e. the rated input power. Heat and cold from conventional technologies are provided via dedicated connections and are always available to all the clusters.

• *Heat pump.* This generates heat by using electricity and by

**Table 1**

Technology and network parameters with reference to the Anergy Grid of ETH Zurich, see Fig. 1. A different number of boreholes,  $n$  is installed in the different geothermal fields, namely 101 (HPL), 128 (HC) and 200 (HWO). The profiles of heat and cold demands of the different clusters are reported in Fig. S1 in the Appendix A.

Quantity		Unit	Value
<i>Central generation (HEZ)</i>			
Boiler efficiency,	$\eta$	–	0.92
Chiller efficiency,	$\eta$	–	3.5
<i>Demand Clusters</i>			
Cooling low temperature,	$T_{LT}^c$	°C	12
Cooling high temperature,	$T_{HT}^c$	°C	16
Heat pump performance parameter,	$\eta_1$	–	6.493
Heat pump performance parameter,	$\eta_2$	kW/°C	5.285
Heat pump performance parameter,	$\eta_3$	kW	–36.1
Heat pump performance parameter,	$\beta_1$	s/ kg	1.063
Heat pump performance parameter,	$\beta_2$	–	–0.006
Heat pump power parameter,	$\delta$	–	0.1
HWTS self-discharge efficiency,	$\Lambda$	1/ h	0.005
HWTS ambient loss contribution coefficient,	$\Pi$	–	0.001
HWTS charging efficiency,	$\eta^{\text{in}}$	–	0.95
HWTS discharging efficiency,	$\eta^{\text{out}}$	–	0.95
HWTS charging/discharging time,	$\tau$	h	3
<i>Water network</i>			
Specific heat of water,	$c$	kJ/ (kg K)	4.186
Minimum mass flow rate,	$m^{\text{min}}$	kg/s	0
Maximum mass flow rate,	$m^{\text{max}}$	kg/s	80
<i>Geothermal fields</i>			
Undisturbed soil temperature,	$T^0$	°C	14
Soil thermal conductivity,	$\lambda$	W/ (K m)	1.8
Soil thermal diffusivity,	$\alpha$	m <sup>2</sup> /s	$5.1 \cdot 10^{-7}$
Euler-Mascheroni constant,	$\gamma$	–	0.577
Borehole thermal resistance,	$R^b$	(m K)/ W	88
Length of borehole heat exchangers,	$L$	m	400
Minimum temperature,	$T^{\text{min}}$	°C	8
Maximum temperature,	$T^{\text{max}}$	°C	24

decreasing the temperature of the water transiting through the demand cluster (see Fig. 2). For all clusters  $i \in \mathcal{D}$ , the generated thermal power,  $P_{t,i}$ , the absorbed electrical power,  $F_{t,i}$ , the mass flow rate of the water circulating through the heat pump,  $m_{t,i}$  and its temperatures,  $T_{t,i}^{\text{in}}$  and  $T_{t,i}^{\text{out}}$ , are computed as

$$P_{t,i} = \eta_{t,i} F_{t,i} \quad (4)$$

$$P_{t,i} = F_{t,i} + cm_{t,i}(T_{t,i}^{\text{in}} - T_{t,i}^{\text{out}})x_{t,i} \quad (5)$$

$$\delta S_i x_{t,i} \leq F_{t,i} \leq S_i x_{t,i} \quad (6)$$

Here,  $x_{t,i}$  is a binary variable indicating whether the heat pump of cluster  $i$  is turned on at time interval  $t$ , producing power but also incurring in a minimum power consumption  $\delta S_i$ ;  $c$  is the specific heat of water. The conversion efficiency,  $\eta_{t,i}$ , is a function of the heat pump operating temperatures as

$$\eta_{t,i} = \frac{T^{\text{cond}}}{T^{\text{cond}} - T_{t,i}^{\text{eva}}} \xi \quad (7)$$

where  $\xi$  is the Carnot efficiency;  $T^{\text{cond}}$  is the heat pump condensation temperature, which is defined by the heat demand and considered to be constant at 40 °C.  $T_{t,i}^{\text{eva}}$  is the heat pump evaporation temperature, which is a function of the inlet and outlet temperatures of the water going through the heat pump, and is computed by

$$T_{t,i}^{\text{out}} = T_{t,i}^{\text{in}} - (T_{t,i}^{\text{in}} - T_{t,i}^{\text{eva}}) \left[ 1 - \exp\left(-\frac{UA}{cm_{t,i}}\right) \right] x_{t,i} \quad (8)$$

where  $U$  is the overall heat transfer coefficient and  $A$  the heat exchange area of the evaporator.

• *Heat exchanger.* This is modeled as a counter-current heat exchanger that provides the cooling power  $P_{t,i}$ , at temperature  $T_{t,i}^{\text{in}}$ , according to

$$P_{t,i} = cm_{t,i}(T_{t,i}^{\text{out}} - T_{t,i}^{\text{in}})x_{t,i} \quad (9)$$

where

$$0 \leq P_{t,i} \leq S_i \quad (10)$$

Here,  $x_{t,i}$  is a binary variable enabling the bypass of the heat exchanger when the inlet temperature exceeds the value specified by the demand cluster,  $T^c$ :

$$T_{t,i}^{\text{in}} \leq T^c \quad (11)$$

Two heat exchangers, characterized by two different values of  $T^c$ , are present in the Anergy Grid of ETH Zurich (see Section 2).

• *Geothermal field.* The heat diffusion through the soil is studied by modeling the boreholes as infinite line heat sources. Assuming a homogeneous soil with constant properties, the temperature distribution resulting from each borehole is given by the solution reported by Carslaw and Jaeger, who determined the dynamic response of the ground temperature to a constant heat step [54]. This is usually referred to as the g-function,  $g$ , or the dimensionless temperature response factor, of the borehole [55], and it can be approximated by a logarithmic function of time that depends on the geometry of the borehole (i.e. depth and radius) and the properties of the soil (i.e. thermal diffusivity and conductivity):

$$g_b(r, t) = \log\left(\frac{4\alpha t}{r^2}\right) - \gamma \quad (12)$$

where  $r$  is the radius of the borehole and  $t$  the time instant;  $\alpha$  is the thermal diffusivity of the soil and  $\gamma$  the Euler-Mascheroni constant; the subscript "b" indicates that Eq. (12) applies to a single borehole. The g-function is computed with hourly resolution along

the time horizon of one year. Later, more accurate numerical solutions [56–59] and analytical approximations [60,61] were presented.

The geothermal fields are modeled by considering the thermal interference among individual boreholes. More specifically, we adopt the spatial superposition principle proposed in references [62,58], which results in an aggregated dynamic response of the overall geothermal fields, i.e. the  $g$ -function appearing hereafter and shown in Fig. S3 in Appendix B. This depends on the properties of the soil and on the geometry of the field (i.e. depth, radius and location of the boreholes). Furthermore, since the aggregated  $g$ -function describes the thermal response of the geothermal field to a heat step, the time varying heat injection/extraction is modeled through the temporal superposition of several heat steps. Therefore, the average temperature of the  $j$ -th geothermal field,  $\forall j \in \mathcal{J}$ , is described as follows [63,64]:

$$T_{t,j} = T^0 + \frac{1}{2\pi\lambda L n_j} \sum_{k=1}^t (Q_{k,j} - Q_{k-1,j}) g(r_j, t - k) \quad (13)$$

where  $T^0$  is the undisturbed soil temperature,  $\lambda$  the thermal conductivity of the ground,  $L$  the length of the borehole heat exchangers (twice the depth of the geothermal fields),  $n_j$  the number of boreholes, and  $r_j$  the radius of the geothermal field;  $Q$  indicates the net injected thermal power, i.e.  $P - F$ , which is positive if heat is extracted and negative if heat is injected. The same depth and properties of the soil are considered for all geothermal fields, whereas these can differ in terms of radius and number of boreholes. The net injected thermal power is expressed as

$$Q_{t,j} = cm_{t,j}(T_{t,j}^{\text{out}} - T_{t,j}^{\text{in}}) \quad (14)$$

where  $m$ ,  $T_{t,j}^{\text{in}}$  and  $T_{t,j}^{\text{out}}$  are the mass flow rate, inlet and outlet temperature of the water circulating through the geothermal field. The energy balance at the wall of a single borehole allows to write

$$\frac{Q_{t,j}}{Ln_j} = \frac{1}{R^b} (T_{t,j} - T_{t,j}^w) \quad (15)$$

where  $R^b$  is the thermal resistance of the borehole and  $T_{t,j}^w$  the water average temperature, which is approximated as the average between the inlet and outlet water temperatures. The model of the geothermal field is validated using the measurements shown in Fig. S2 in Appendix B.

Within the system optimization, the temperature of the geothermal fields is constrained between a minimum and a maximum value because of environmental limitations:

$$T^{\min} \leq T_{t,j} \leq T^{\max} \quad (16)$$

Furthermore, a periodicity constraint is imposed on the geothermal fields. This forces the same field temperature at the beginning and at the end of the year, thus enabling a sustainable field operation across the years,

$$T_{0,j} = T_{N,j} \quad (17)$$

- **Hot water thermal storage (HWTS).** This type of thermal storage is the cheapest and most deployed thermal storage technology. Due to its high energy losses and low energy density, HWTS is mostly used to offset short-term mismatch between thermal energy generation and use. For all clusters  $i \in \mathcal{C}$ , the energy stored within the HWTS,  $E_{t,i}$ , is expressed through the following linear dynamics [49]

$$E_{t,i} = E_{t-1,i}(1 - \Lambda\Delta t) - \left( \Pi S_i h_t + \eta^{\text{in}} F_{t,i} - \frac{1}{\eta^{\text{out}}} P_{t,i} \right) \Delta t \quad (18)$$

where

$$E_{0,i} = E_{N,i} \quad (19)$$

$$h_t = \frac{T^{\min} - T_t^{\text{amb}}}{T^{\max} - T^{\min}} \quad (20)$$

$$0 \leq E_{t,i} \leq S_i \quad (21)$$

$$-\frac{S_i}{\tau} \leq F_{t,i}, P_{t,i} \leq \frac{S_i}{\tau} \quad (22)$$

Here,  $\Lambda$  and  $\Pi$  are self-discharge parameters, and  $h_t$  expresses the influence of ambient temperature on the energy losses of the storage unit, as suggested in [65];  $\eta^{\text{in}}$  and  $\eta^{\text{out}}$  indicate the charging and discharging efficiency, respectively;  $\Delta t$  is the duration of the  $t$ -th time interval (between time steps  $t - 1$  and  $t$ );  $\tau$  is the time required to fully charge or discharge the storage. Here, we consider water stored at  $T^{\max} = 55$  °C and cooled to  $T^{\min} = 40$  °C. Also, we consider the same value for charging and discharging efficiency. The periodicity constraint, Eq. (19), imposes the same storage level at the beginning and at the end of the yearly time horizon.

(II) **Thermal network mass and energy balances.** The mass and energy balances are defined for all intersection points of the thermal network, as well as for the demand clusters.

- **Network mass and energy balances.** Each intersection point in the thermal network is a connection of three branches, which are in turn connected to three different nodes (with references to Section 3.2,  $\mathcal{B} = \{1, 2, 3\}$ ). Each node can be a cluster, a geothermal field, or another intersection point. The mass balance for the  $i$ -th intersection point,  $\forall i \in \mathcal{I}$ , is

$$\sum_{l=1}^3 d_{t,i,l} m_{t,i,l} = \sum_{l=1}^3 (1 - d_{t,i,l}) m_{t,i,l} \quad (23)$$

where  $m_{t,i,l}$  is the mass flow rate of the water entering or exiting the intersection point  $i$  through the branch  $l$  at time interval  $t$ ;  $d_{t,i,l}$  is a binary variable specifying whether the water flow is entering ( $d = 1$ ) or exiting ( $d = 0$ ) the intersection point. The maximum value of mass flow rate circulating inside each branch is reported in Table 1.

The energy balance for the  $i$ -th intersection point is

$$\sum_{l=1}^3 d_{t,i,l} m_{t,i,l} T_{t,i,l}^{\text{out}} = \sum_{l=1}^3 (1 - d_{t,i,l}) m_{t,i,l} T_{t,i,l}^{\text{in}} \quad (24)$$

$$y_{t,i} [d_{t,i,l} T_{t,i,l}^{\text{out}} + (1 - d_{t,i,l}) T_{t,i,l}^{\text{in}}] = \gamma_{t,i}, \quad l = \{1, 2, 3\} \quad (25)$$

where

$$y_{t,i} = 2 - \sum_{l=1}^3 d_{t,i,l} \quad (26)$$

where Eq. (25) imposes that, in the case of an entering flow being split into two exiting flows, the temperatures of all flows are the same; Eq. (26) defines the binary variable  $y_{t,i}$ , which states whether a node mixes two flows ( $y_{t,i} = 0$ , i.e. the temperature of each branch is defined by Eq. (24)) or split one flow ( $y_{t,i} = 1$ , i.e. all branches are at the same temperature).

- **Cluster energy balance.** The energy balance within the  $i$ -th cluster states that the generated energy must equal the energy demand for each energy carrier  $j \in \mathcal{C}$ . This is expressed as

$$\sum_{k \in \mathcal{C}} (P_{t,i,k,j} - F_{t,i,k,j}) - D_{t,i,j} = 0 \quad (27)$$

where  $P_{t,i,k,j}$  and  $F_{t,i,k,j}$  are the produced and consumed power of



carrier  $j$  by technology  $k$  in cluster  $i$  at time interval  $t$ ;  $D_{t,i,j}$  is the demand required by the end-users. Eq. (27) states that the power demand of each cluster must be satisfied exactly, which represents the reference case for our analysis. However, the Energy Grid system allows for the flexibility to produce power beyond the demand and to release the excess power to the environment (i.e. to dissipate energy), if this improves the value of the objective function. In this case, Eq. (27) is replaced by the following equations

$$\sum_{k \in \mathcal{K}} (P_{t,i,k,j} - F_{t,i,k,j}) - D_{t,i,j} \geq 0 \quad (28)$$

$$\sum_{t=1}^N \sum_{i \in \mathcal{I}} \sum_{j \in \mathcal{J}} \left[ \sum_{k \in \mathcal{K}} (P_{t,i,k,j} - F_{t,i,k,j}) - D_{t,i,j} \right] \leq \phi \sum_{t=1}^N \sum_{i \in \mathcal{I}} \sum_{j \in \mathcal{J}} D_{t,i,j} \quad (29)$$

where  $\phi$  is defined as the amount of energy that can be released to the environment normalized over the total annual energy demand ( $\sum_{t=1}^N \sum_{i \in \mathcal{I}} \sum_{j \in \mathcal{J}} D_{t,i,j} \Delta t$ ).

### 3.4. Objective function

The objective function to be minimized is given by the annual CO<sub>2</sub> emissions of the system,  $e$ . These are due to electricity and natural gas imported from the distribution grids to run the heat pumps and the centralized chiller and boiler. They are expressed as

$$e = \sum_{j \in \mathcal{J}} \epsilon_j \sum_{i \in \mathcal{I}} \sum_{k \in \mathcal{K}} \sum_{t=1}^N F_{t,i,k,j} \Delta t \quad (30)$$

where  $\epsilon_j$  is the carbon intensity (inclusive of the entire life cycle) of carrier  $j$ . Here, the carbon intensity of electricity and natural gas are  $\epsilon_e = 30 \text{ g}_{\text{CO}_2}/\text{kWh}$  (corresponding to the life cycle assessment emissions of low-carbon electricity produced by renewable energy sources) and  $\epsilon_g = 237 \text{ g}_{\text{CO}_2}/\text{kWh}$ , respectively.

## 4. Optimization strategy

We aim at minimizing the CO<sub>2</sub> emissions of the system while satisfying the heating and the cooling demands. To do so, we determine the hourly scheduling (ON/OFF) and operations of the heat pumps and of the heat exchangers for the five demand clusters, the heat exchanged

with the three geothermal fields and their temperature evolution, and the temperature and mass flow rate profiles for all branches of the network. The implemented optimization procedure, illustrated in Fig. 3, proceeds as follows:

(1) A MINLP problem is formulated that describes the nonlinear behavior of the system, i.e. Eqs. (2)–(30). Two major sources of nonlinearity are (i) the efficiency of the heat pumps, given by Eqs. 4, 7, 8, which is a nonlinear function of inlet and outlet temperatures, and (ii) the energy output of the heat exchangers, which is proportional to the product of mass flow rate and temperature (i.e. product of decision variables). The dynamic response of the geothermal fields (i.e. the g-function) is a known quantity, not subject to optimization, and therefore does not introduce nonlinearities. Also, the nonlinearities arising from the product of continuous and binary decision variables can be eliminated by reformulating them as combination of linear constraints [66].

(2) The MINLP problem formulated in (1) cannot be solved efficiently due to the large number of decision variables for this class of mathematical optimization problems. Therefore, it is relaxed into a MILP problem by (i) defining a linear approximation of the heat pump performance described by Eqs. 4, 7, 8, and (ii) adopting a linear relaxation of the heat exchange model in Eqs. 5, 9, 14, 24. For the heat pumps, Eqs. 4, 7, 8 are replaced by the following linear approximations:

$$P_{t,i} = \eta_1 F_{t,i} + (\eta_2 T_{t,i}^{\text{in}} + \eta_3) x_{t,i} \quad (31)$$

$$T_{t,i}^{\text{out}} = T_{t,i}^{\text{in}} - (T_{t,i}^{\text{in}} - T_{t,i}^{\text{eva}})(\beta_1 m_{t,i} + \beta_2) x_{t,i} \quad (32)$$

For the heat exchange, the product  $mT$  appearing in Eqs. 5, 9, 14, 24 is written through its McCormick relaxation [67,68], i.e. by introducing an auxiliary variable  $\tilde{m} = mT$ , which is bounded between the minimum and the maximum value of the product itself. Namely, the equality constraints involving  $mT$  are replaced by inequality constraints involving  $\tilde{m}$ . This represents the most relevant source of nonlinearity. The resulting MILP, which is hereafter referred to as the *relaxed MILP*, is then solved. The flow direction in all the network branches is optimized but remains constant during the year so as to reduce the computational complexity of the problem.

(3) The relaxed MILP has a greater feasibility space than the original

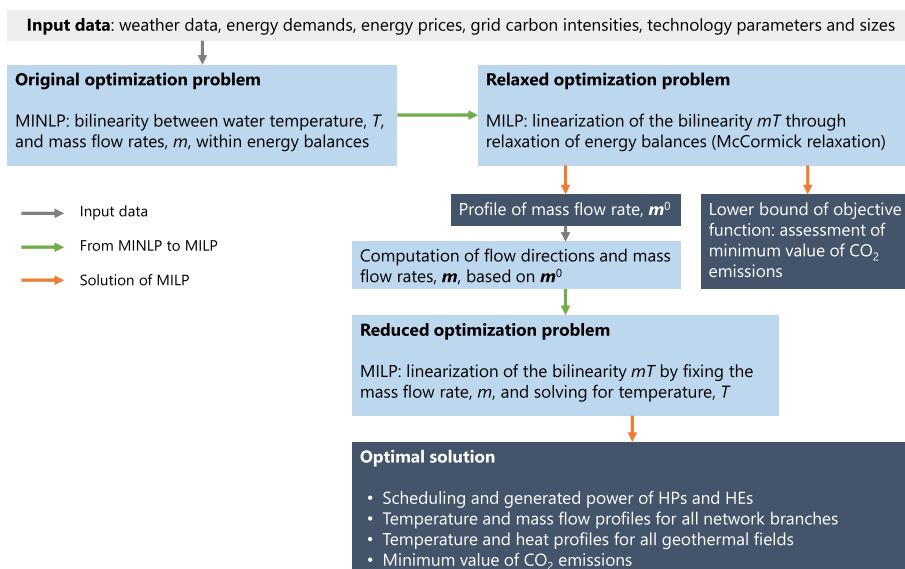


Fig. 3. Summary of the optimization procedure developed to determine the system operation that minimizes CO<sub>2</sub> emissions while satisfying the energy demands.

MINLP, which implies that (i) the solution of the relaxed MILP might be unfeasible when used as input to the original MINLP, and (ii) the optimal values of the objective function of the MILP is lower than or equal to that of the MINLP, i.e. the value of CO<sub>2</sub> emissions of the system cannot be lower than that found through the relaxed MILP. The relaxed MILP is solved by modeling the yearly time horizon through ten typical days. This value is chosen after a sensitivity analysis showing deviations smaller than 1% with respect to the full-resolution optimization for a number of typical days greater than eight. The value of 1% represents the MIP gap of the MILP, which defines the precision of the optimal solution.

(4) The profile of mass flow rate obtained through the relaxed MILP, denoted as  $m^0$ , describes the time evolution of the mass flow rate within the clusters, the geothermal fields and the network branches. However, we note this solution generally underestimates the optimal value of the mass flow rate, because it selects the lower bound identified by the McCormick inequality constraints imposed on  $\tilde{m}$ . Therefore, we determine the actual mass flow rate circulating through the thermal network, denoted as  $m$ , by increasing the value of  $m^0$  through three different heuristic approaches:

- (i) by replacing  $m^0$  with a higher constant value  $\nu$ , i.e.  $m_t = \nu, \forall t \in \{1, \dots, N\}$ ;
- (ii) by scaling up  $m^0$  through a constant multiplication factor  $\zeta$ , i.e.  $m_t = m_t^0 \zeta, \forall t \in \{1, \dots, N\}$ ;
- (iii) by shifting  $m^0$  through a constant additive factor  $\kappa$ , i.e.  $m_t = m_t^0 + \kappa, \forall t \in \{1, \dots, N\}$ .

The profile of mass flow rate obtained in this way is fixed and used as an input to the original MINLP problem, resulting in a *reduced MILP* having only temperatures as decision variables. The results in Section 5 are obtained by solving this reduced MILP, which is the ultimate end point of the optimization procedure.

To compare the different heuristic approaches, we introduce the normalized average mass flow rate,  $\mu$ , which is the ratio of the average value of  $m$  to the average value of  $m^0$ :

$$\mu = \frac{\sum_{t=1}^N m_t}{\sum_{t=1}^N m_t^0} \quad (33)$$

For the three heuristic approaches introduced above  $\mu$  is expressed as

$$(i) \quad \mu = \frac{N\nu}{\sum_{t=1}^N m_t^0} \quad (34)$$

$$(ii) \quad \mu = \zeta \quad (35)$$

$$(iii) \quad \mu = \frac{N\kappa}{\sum_{t=1}^N m_t^0} + 1 \quad (36)$$

where larger values of  $\nu$ ,  $\zeta$  and  $\kappa$  result in larger values of mass flow rate and therefore  $\mu$ .

(5) The solution of the reduced MILP returns the minimum value of CO<sub>2</sub> that can be attained and the corresponding optimal operation strategy. This is given by the time evolution of (i) the scheduling and the generated power of heat pumps and heat exchangers, (ii) the heat injected/extracted to/from the geothermal fields, (iii) the temperature of the geothermal fields, (iv) the mass flow profiles across the network.

The optimization problem is formulated in Matlab [69] by using the YALMIP interface [70]. The reduced MILP is solved by using CPLEX 12.8.0 [71], set to have a relative MIP gap of 1%.

## 5. Results and discussion

First, the results of the analysis are described and discussed by referring to a single demand cluster connected to a single geothermal field, namely the HPL demand cluster and the HPL geothermal field. This allows deriving general trends valid for all demand clusters and helps understanding the behavior of the entire Energy Grid of ETH Zurich, which is then presented.

The scope of the analysis is to determine the operation strategy that minimizes the CO<sub>2</sub> emissions of the system. To this end, we identify the most relevant operation and design quantities and we investigate their optimal values. The most relevant quantities prove to be the mass flow rate circulating through the thermal network, the minimum-power fraction of the heat pump, the presence of hot water thermal storage, the operation of the conversion technologies (i.e. heat pump and heat exchangers), and the possibility of dissipating energy to the environment. Overall, the CO<sub>2</sub> emissions are minimized when the system

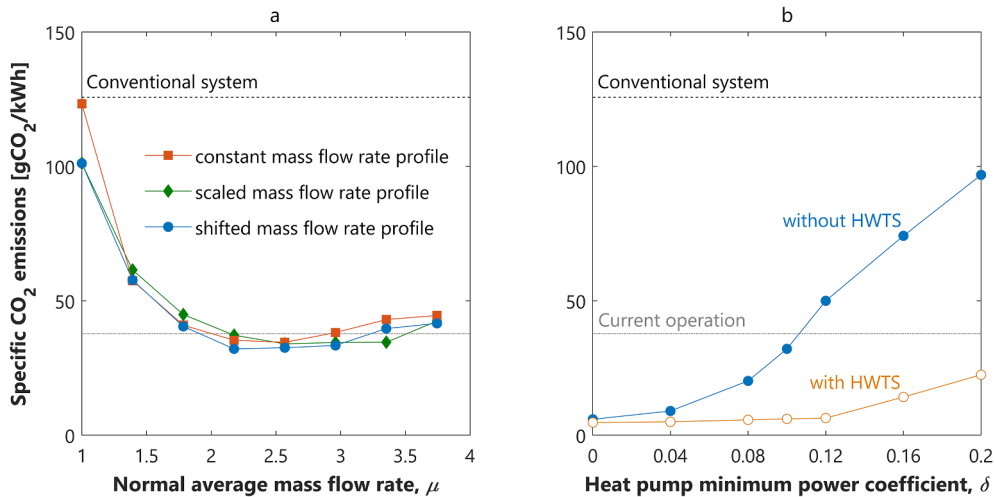


Fig. 4. Specific CO<sub>2</sub> emissions of the HPL demand cluster as function of (a) normalized average mass flow rate circulating in the network,  $\mu$ , and (b) minimum-power fraction of the heat pump,  $\delta$ , and of the presence of hot water thermal storage, HWTS. Three different mass flow rate profiles are shown in (a), corresponding to the three strategies introduced in Section 4. A shifted mass flow rate profile with  $\mu = 2.18$ , which enables the lowest value of CO<sub>2</sub> emissions, is used in (b).

flexibility is maximized, i.e. when the thermal network is able to meet both the heating and cooling demands at the same time.

### 5.1. HPL demand cluster and geothermal field

The system showed in Fig. 2 is considered, where the water circulating through the cluster substation (i.e. heat pump and heat exchangers) comes from and goes to a geothermal field. This describes the HPL demand cluster connected to the HPL geothermal field. The flow direction in the network is fixed, with the following steps: a given mass flow rate,  $m$ , leaves the geothermal field at temperature  $T_1$ ; the water decreases its temperature by going through the HP, if this is ON, or it maintains the same temperature by bypassing it, if this is OFF, hence  $T_2 \leq T_1$ ; the water increases its temperature by going through the LTHE, if this is ON, or it maintains the same temperature by bypassing it, if this is OFF, hence  $T_3 \geq T_2$ ; the same applies to the HTHE, hence  $T_4 \geq T_3$ ; the water increases or decreases its temperature by going through the boreholes of the geothermal field, depending on the field temperature (see Eqs. (13)–(15)).

#### 5.1.1. Minimum CO<sub>2</sub> emissions

Fig. 4 shows the specific CO<sub>2</sub> emissions of the system as function of the mass flow rate circulating in the network,  $\mu$  ( Fig. 4-a), of the minimum-power fraction of the heat pump,  $\delta$ , and of the presence of hot water thermal storage, HWTS ( Fig. 4-b), which have proved to be the most relevant quantities to determine the minimum attainable value of CO<sub>2</sub> emissions of the single HPL cluster. The specific CO<sub>2</sub> emissions are normalized over the total annual heating and cooling demand, and the normalized average mass flow rate is used to express the mass flow rate (see Eq. (33) in Section 4). For comparison, Fig. 4 reports (i) the value of CO<sub>2</sub> emissions of the HPL demand cluster obtained by using the centralized heating and cooling technologies, without deploying the thermal network (horizontal black dashed line), and (ii) the value of CO<sub>2</sub> emissions of the HPL demand cluster achieved with the current operation (horizontal gray dotted-dashed line) [72,42]. Fig. 4-a reports the CO<sub>2</sub> emissions obtained when fixing the mass flow rate through the three heuristic approaches described in Section 4, which are indicated by (i) the orange squares – constant mass flow rate, (ii) the green diamonds – time-dependent mass flow rate, and (iii) the blue circles – time-dependent mass flow rate. Two main considerations can be made. First, a time-dependent mass flow rate results in lower values of the CO<sub>2</sub>

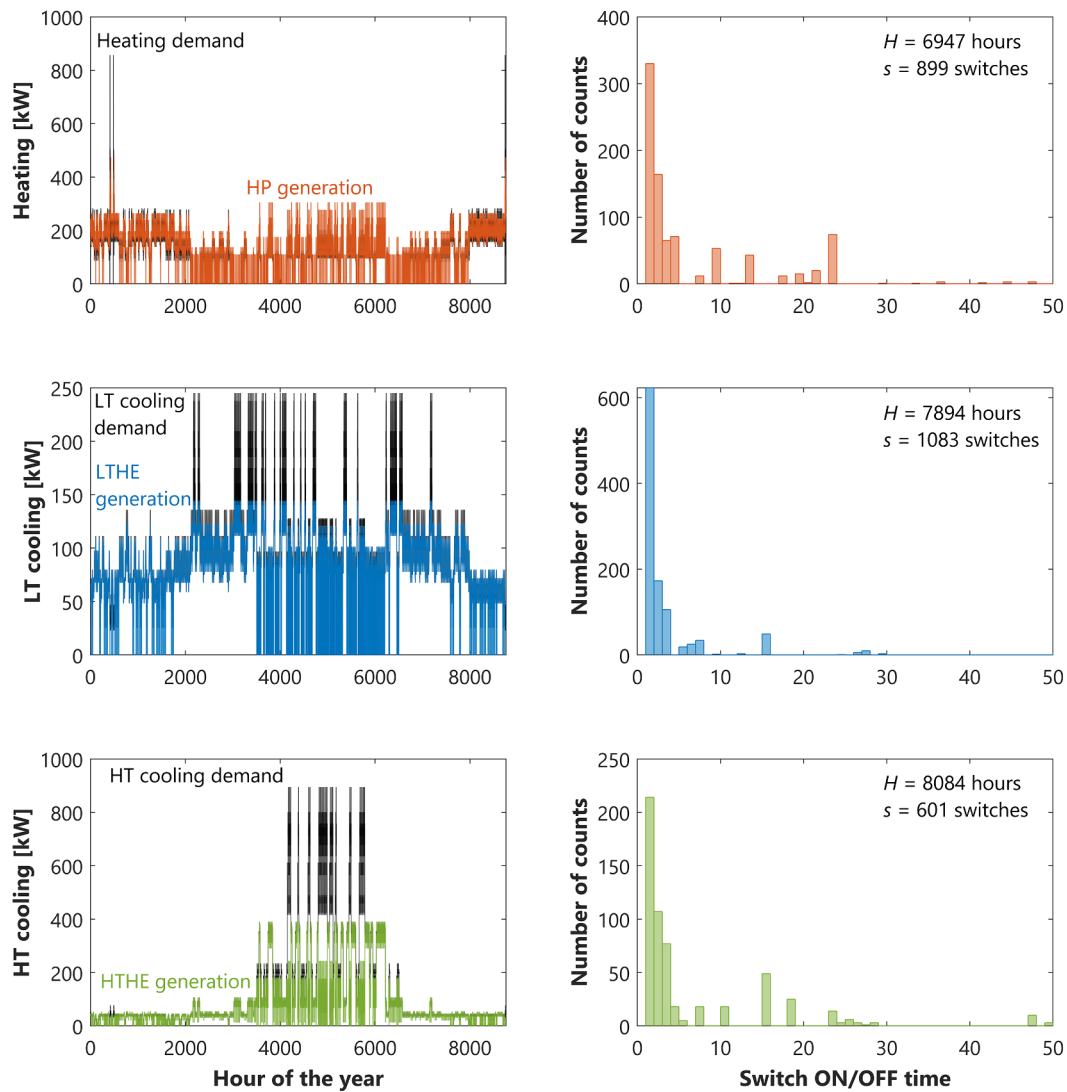


Fig. 5. Optimal operation of HPL demand cluster. Time profiles of energy generation (left) and number of counts of ON/OFF switch times (right) for heating, LT cooling and HT cooling. Heating is supplied via HP, LT cooling via LTHE, and HT cooling via HTHE. On the left, the energy generation is superposed to the corresponding energy demand (transparent). On the right, the number of yearly operating hours,  $H$ , and the number of yearly switches,  $s$ , are reported. Shifted mass flow rate profile with  $\mu = 2.18$  and  $\delta = 0.1$ .

emissions, as it allows following the time evolution of heating and cooling demands. In fact, the differences between the three strategies are small, as the system can adapt to different mass flow rates via different technology operations, as detailed in the following. Second, for all approaches there is an optimal value of  $\mu$  (i.e. an optimal value of average mass flow rate) that minimizes the CO<sub>2</sub> emissions. This stems from the trade-off between low values of mass flow rate, for which only a small fraction of the energy demand is satisfied, and high values of mass flow rate, for which the heating and cooling demands cannot be satisfied at the same time because one of the two would be exceeded (and no partial bypass is allowed by the system). To clarify this concept, consider a high value of water mass flow rate during a time of the year in which the heating demand is higher than the cooling one (e.g. autumn). The water would circulate through the heat pump, hence meeting the heating demand; however, it would bypass the heat exchangers (as too much cooling would be provided), hence not providing any cooling. Similar considerations hold true when the cooling demand is higher than the heating one. Hereafter, we use strategy (iii) to fix the water mass flow rate, as it results in the lowest values of CO<sub>2</sub> emissions and allows operating the system with the lowest mass flow rates. Fig. 4-b shows the impact of the HP minimum-power fraction on the total CO<sub>2</sub> emissions of the system (see Eq. (6)). The same analysis is performed with and without the possibility of installing the HWTS. The value of  $\delta$  identifies the minimum heating demand that can be satisfied by the heat pump; lower values of  $\delta$  imply the possibility of covering a wider range of heating demand and result in lower CO<sub>2</sub> emissions. From a design perspective, this allows quantifying the advantage of having a modular heat pump installation (lower minimum-power fraction) over having a unique technology (higher minimum-power fraction).

Deploying the HWTS allows to reduce the CO<sub>2</sub> emissions at high values of  $\delta$ , where the storage system is needed to satisfy heating demands smaller than the HP minimum-power fraction. The larger the value of  $\delta$ , the larger the fraction of heating demand satisfied by the HWTS, the larger the benefit in terms of CO<sub>2</sub> emissions; when  $\delta = 0$  there is no advantage in installing the HWTS, since the HP can cover the entire range of heating demand. Overall, the short-term flexibility provided by the storage system allows to (i) operate the HP during more hours of the year, and (ii) directly compensate the mismatch between heat generation and demand. HWTS is a mature and relatively cheap technology, which makes its installation a low hanging fruit for

reducing the system's emissions. A reference value of  $\delta = 0.1$  is considered across the paper, which characterizes the technologies installed in the Anergy Grid system [72,42].

### 5.1.2. System operation

Let us now investigate in more detail the optimal operation of the single HPL cluster. Fig. 5 shows the optimal operation of the heat pump and of the heat exchangers during every hour of the year. On the left-hand side we compare the hourly energy production with the corresponding energy demand (transparent). On the right-hand side we show the frequency with which the technologies are switched ON and OFF, by defining the ON/OFF switching time as the number of hours after which a technology changes its status from ON to OFF or viceversa. The yearly operating hours,  $H$ , and the yearly switches,  $s$ , are also reported.

The HP supplies about 98% of the heating demand required by the cluster, either directly or through the HWTS, with the central boiler mostly contributing during the winter peaks. During the year, the heat pump is operated for about 7000 h and it is most often switched ON/OFF every one or two hours, though longer operating periods of about 10 and 20 h are not uncommon. The longest periods without switches last about 800 h, but periods longer than 60 h occur about 20 times per year.

The LTHE supplies about 79% of the LT cooling demand and is operated for about 7900 h. It is most often switched ON/OFF every one or two hours and common operating periods are shorter than 10 h. The longest periods without switches last about 1700 h, but periods longer than 50 h occur about 20 times per year.

Similar considerations can be made for the HTHE, which supplies about 66% of the HT cooling demand, with the central chiller mostly contributing during the summer peaks. It is most often switched ON/OFF every one, two or three hours, but longer operating periods up to 30 h are not uncommon. The longest periods without switches last about 1100 h, but periods longer than 70 h occur about 20 times per year.

Furthermore, the relatively low coverage of cooling demand demonstrates that the heating demand is the major responsible for CO<sub>2</sub> emissions. This is because conventional heat generation is based on natural gas, while conventional cold generation is based on electricity coming from renewable energy sources [73].

The optimal behavior of the storage systems is illustrated in Fig. 6, which shows (a) the temperature profile and the extracted/injected heat of the geothermal field and (b) the energy stored within the HWTS.

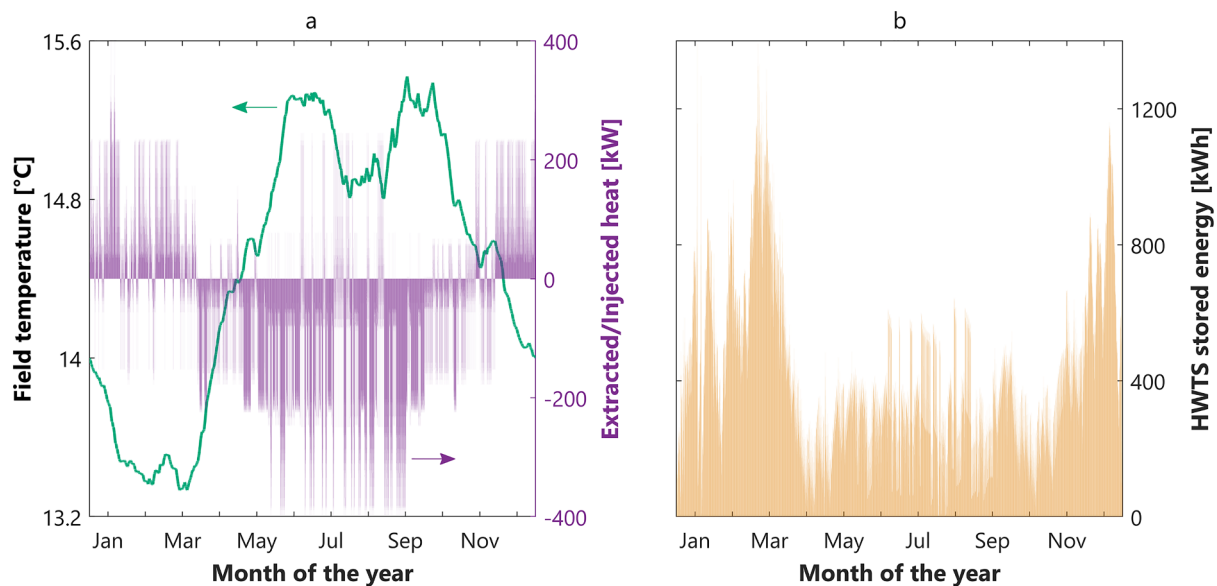


Fig. 6. Optimal storage operation for the HPL demand cluster. (a) Optimal temperature profile of the geothermal field (green line - left vertical axis) and of the extracted/injected heat (positive/negative values of the purple line - right vertical axis). (b) Optimal profile of stored energy within HWTS. Shifted mass flow rate profile with  $\mu = 2.18$  and  $\delta = 0.1$ . (For interpretation of the references to colour in this figure legend, the reader is referred to the web version of this article.)

In Fig. 6-a the heat (purple line – right vertical axis) is positive when extracted from the ground (the water circulating through the geothermal field is heated up) and negative when injected into the ground (the water circulating through the geothermal field is cooled down). Heat is extracted during winter, which results in a decreasing temperature of the geothermal field (green line – left vertical axis), and is injected during summer, which results in an increasing temperature of the geothermal field. Two distinct temperature peaks are observed in summer following two greater heat injections. After these, the temperature tends to settle to the undisturbed value of 14 °C. The periodicity constraint given by Eq. (17) imposes that the field temperature at the beginning and at the end of the year is equal to the undisturbed value, hence constraining the heat extraction/injection and ensuring a long-term sustainable operation of the field. Fig. 6-b shows the operation of the HWTS. While this is mostly used to compensate the short-term mismatch between heat generation and demand, longer storage cycles are observed in winter, where heat storage is most needed. This increases the flexibility of the heat pumps, which can operate also when no heat is required. Furthermore, it complements the use of the geothermal field, which is intrinsically more suited to compensate longer-term, i.e. seasonal mismatches between energy generation and demand because of its slower storage dynamics.

### 5.2. Entire Energy Grid of ETH Zurich

The analysis performed in Section 5.1 for the HPL cluster and geothermal field is applied to the entire network shown in Fig. 7, which describes the Anergy Grid of ETH Zurich, and where the blue and red arrows indicate the direction of the water flowing in the network branches, which is optimized but remains constant during the year. All demand clusters are modeled as described for the HPL cluster, i.e. series of HP, LT and HT, with the possibility of storing heat in the HWTS. Here we do not present the impact of the HP minimum-power fraction, which is similar for all clusters, but we present and discuss the possibility of dissipating energy to the environment, i.e. of exceeding the energy demands, which becomes more relevant when optimizing the entire system.

#### 5.2.1. Minimum CO<sub>2</sub> emissions

Fig. 8 shows the specific CO<sub>2</sub> emissions of the entire system as function of the normalized average mass flow rate circulating in the network,  $\mu$  ( Fig. 8-a), of the amount of energy dissipated to the environment,  $\phi$  (see Eqs. (28) and (29)), and of the presence of HWTS (Fig. 8-b). The value of  $\mu$  is calculated by considering all the branches of the thermal network. For comparison, Fig. 8 reports (i) the value of CO<sub>2</sub> emissions of the Anergy Grid obtained by using the centralized heating and cooling technologies, without deploying the thermal network (horizontal black dashed line), and (ii) the value of CO<sub>2</sub> emissions of the Anergy Grid achieved with the current operation (horizontal gray dotted-dashed line) [72,42]. Currently the system is operated by following seasonal patterns, with heat pumps and heat exchangers determining the operation in winter and summer, respectively.

In the Anergy Grid of ETH Zurich, energy dissipation to the environment is permitted and represents an additional form of flexibility, which allows (i) to satisfy a higher fraction of energy demand via the Anergy Grid by better handling the unbalance between the overall heating and cooling demands of every cluster, and (ii) to balance the heat injection and extraction to and from the geothermal fields, respectively, hence enabling sustainable field operations (i.e. same ground temperature at the beginning and the end of the year, see Eq. (17)). To clarify this concept, consider the same example above, namely a high value of mass flow rate circulating through the network during a time of the year in which the heating demand is higher than the cooling one. With reference to Fig. 2, assume a mass flow rate of 5 kg/s, a temperature variation of 3.6 °C across the heat pump and the heat exchangers, 100 kWh of heating demand, and 10 kWh of LT and HT cooling demands (i.e. 120 kWh of total energy demands). Such mass flow rate and temperature variations result in the production of about 100 kWh of heat and 75 kWh of LT and HT cold. Therefore, we can decide among the following three options for operating the system: (i) satisfying both the heating and cooling demands via the Anergy Grid and release 130 kWh of cold to the environment (65 kWh each of LT and HT cold –  $\phi = 130/120 = 1.1$ ), (ii) only satisfying the heating demand via the Anergy Grid and inject the cold into the geothermal fields ( $\phi = 0$ ), (iii) satisfying both the heating and cooling demands via the

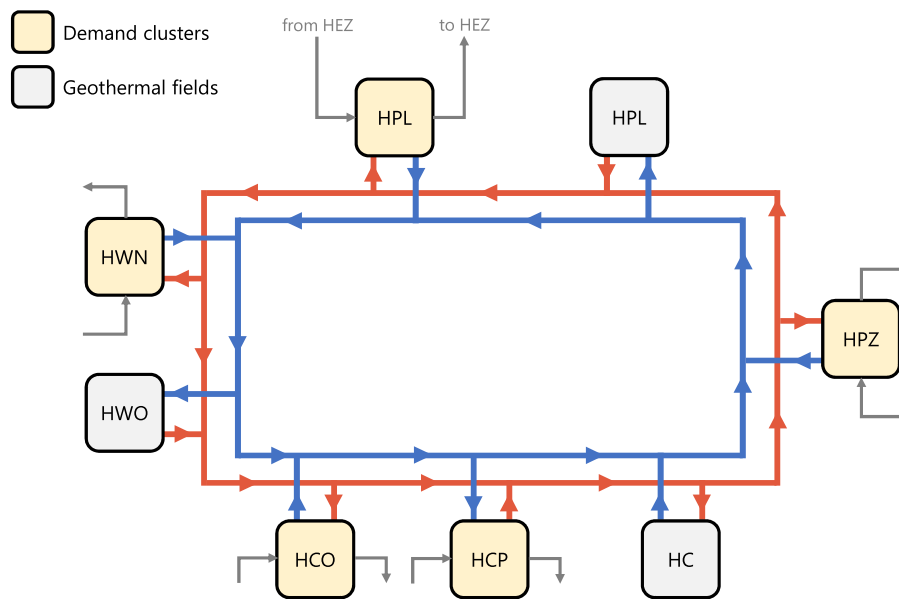
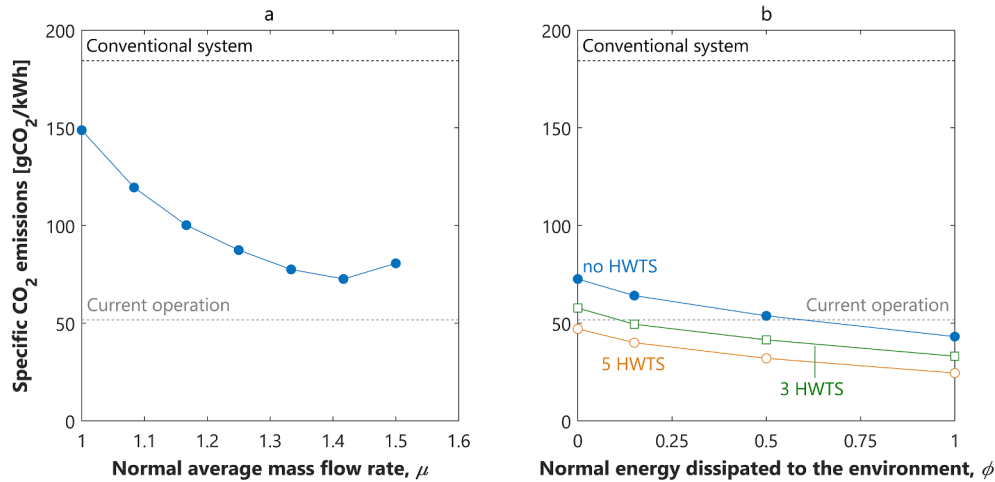


Fig. 7. Schematic of the Anergy Grid of ETH Zurich reporting the demand clusters (yellow) and the geothermal fields (gray). (For interpretation of the references to colour in this figure legend, the reader is referred to the web version of this article.)





**Fig. 8.** Specific CO<sub>2</sub> emissions of the Anergy Grid (AG) of ETH Zurich as function of (a) normalized average mass flow rate circulating in the network,  $\mu$ , and (b) normalized amount of energy dissipated to the environment,  $\phi$ , and of the presence of hot water thermal storage, HWTS. A shifted mass flow rate profile with  $\mu = 1.42$ , which enables the lowest value of CO<sub>2</sub> emissions, is used in (b).

conventional system ( $\phi = 0$ ). The algorithm minimizes the CO<sub>2</sub> emissions by selecting option (ii), as this allows storing the excess energy for later use. However, the prolonged injection of cold into the geothermal field would result in a sustained cooling of the geothermal field, hence provoking a ground temperature at the end of the year lower than at the beginning. This is not compatible with sustainable field operations. When option (ii) is not feasible because it would impair future operations of the geothermal field, the algorithm selects option (i). If option (i) is not feasible (e.g. because no more energy can be released to the environment), the algorithm is forced to select option (iii) resulting in high CO<sub>2</sub> emissions, mostly because the conventional heat generation is based on natural gas. Similar considerations apply when the cooling demand is higher than the heating one. Fig. 8-a reports the CO<sub>2</sub> emissions obtained with  $\phi = 0$  and by fixing the mass flow rate through the heuristic approach (iii) described in Section 4, namely by considering a time-dependent mass flow rate profile computed by shifting up the one obtained with the relaxed MILP optimization problem. When comparing to the single HPL cluster, one can see that (i) smaller values of  $\mu$  are obtained, which means that the optimal value of average mass flow rate (i.e. the value leading to minimum CO<sub>2</sub> emissions) is more similar to the one obtained with the relaxed MILP optimization problem; (ii) overall, larger mass flow rates are circulating into the thermal network, implying that the optimal operation strategy consists in satisfying either the heating or the cooling demand at a given point in time (with one of the two being bypassed); (iii) overall, higher CO<sub>2</sub> emissions can be attained, as a smaller fraction of the overall energy demand is satisfied through the thermal network. This is because the entire system must comply with the constraints of several demand clusters coupled with different geothermal fields and with their simultaneous heating and cooling requirements, which results in a lower flexibility than the case of a single demand cluster exploiting a dedicated geothermal field. Contrary to the single-cluster case, the CO<sub>2</sub> emissions of the system can be reduced with respect to the current operation only by installing HWTS and/or dissipating energy to the environment.

As shown in Fig. 8-b, such emissions are decreased by installing HWTS, with 7% emissions reduction obtained with one HWTS, 19% with three HWTS and 35% with five HWTS (these two cases are reported in Fig. 8-b). Similar to the single cluster, this is because the HWTS enables a wider range of operation for the HP and allows satisfying a larger fraction of the energy demand.

Moreover, a further reduction in CO<sub>2</sub> emissions is achieved by dissipating energy, as this allows to satisfy simultaneously the heating and cooling demands even when one of the two is exceeded. The benefit resulting from dissipating energy (i) does not vary significantly when

increasing the number of installed HWTS, since HWTS is mostly used to meet high energy demands and energy dissipation is mostly used to meet low energy demands; (ii) is greater for the entire system than for the single HPL cluster, where both high and low energy demands can be satisfied via HWTS. A value of CO<sub>2</sub> emissions similar to the current operation is obtained for three HWTS and  $\phi = 0.15$ , i.e. an amount of energy equal to 15% of the total energy demand can be dissipated to the environment. For five HWTS, and for values of  $\phi$  equal to 0.15, 0.5 and 1, a CO<sub>2</sub> emissions reduction of 78%, 83% and 87% is obtained with respect to conventional technologies, respectively (an improvement compared to the value of 72% obtained with the current operation). A value of  $\phi = 1$  results in a system where the excess energy is released to the environment rather than stored underground. The fact that this allows reducing the CO<sub>2</sub> emissions highlights the difficulties in controlling the ground temperature in a sustainable long-term fashion (i.e. same ground temperature is enforced at the beginning and at the end of the year for the sustainability of the geothermal field design) and points towards an optimal expansion of the Anergy Grid where heating and cooling demands are better balanced.

Both CO<sub>2</sub> emissions and operation costs are calculated based on the amount of consumed electricity and natural gas, and therefore a parallel exists between minimizing CO<sub>2</sub> emissions and the operation costs. However, minimizing the CO<sub>2</sub> emissions results in a shift from natural gas to electricity, hence in a higher share of electricity consumption with respect to the conventional system. Considering unit costs of natural gas and electricity equal to 60 EUR/MWh and 120 EUR/MWh, respectively, the conventional system using centralized heating and cooling incurs in operation costs of about EUR 55 per MWh of total energy demand. The proposed optimization strategy allows decreasing the operations to 33 EUR/MWh with three HWTS and  $\phi = 0$ , and to 15 EUR/MWh with five HWTS and  $\phi = 1$ .

### 5.2.2. System operation

The detailed investigation of the optimal operation of the HPL cluster when inserted within the entire Anergy Grid provides additional insights into the management of multi-energy systems coupled with seasonal geothermal energy storage. Compared to the stand-alone operation of the HPL cluster, the conversion technologies are generally operated for less hours during the year and are switched ON and OFF more often, due to the larger average mass flow rates circulating through the network and to the difficulty in simultaneously meeting the heating and energy demands of several clusters.

When resorting to three HWTS and in case of no energy dissipation ( $\phi = 0$ ), the HP supplies about 68% of the heating demand required by

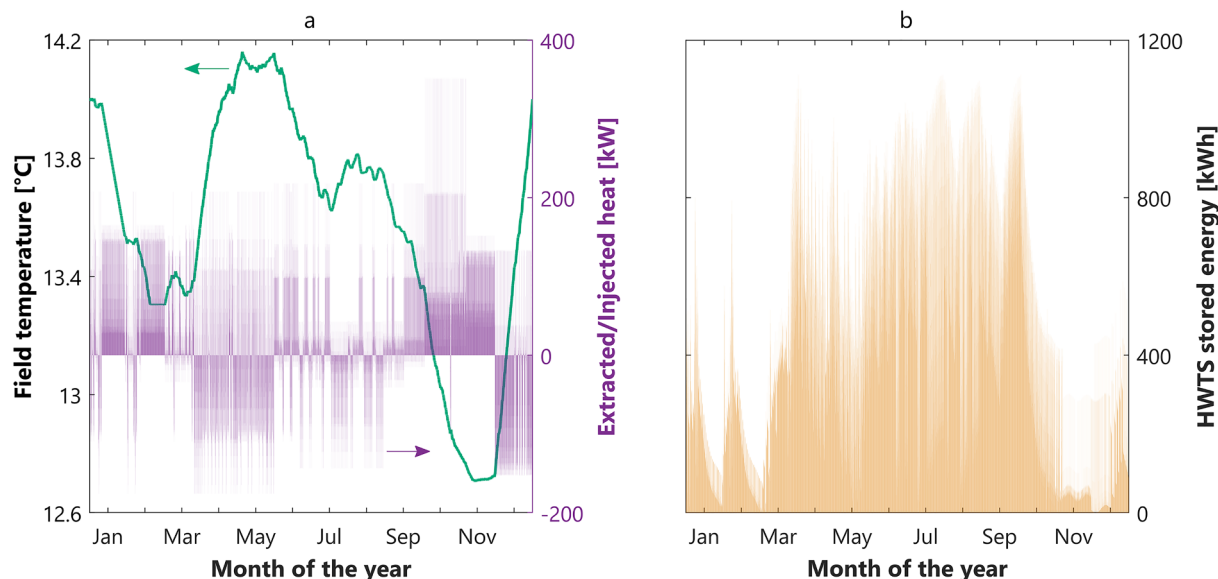


**Fig. 9.** Optimal storage operation of the Anergy Grid of ETH Zurich. (a) Optimal temperature profile of the HPL geothermal field (green line – left y-axis) and of the corresponding extracted/injected heat (positive/negative values of the purple line – right-axis). (b) Optimal profile of stored energy within the HWTS installed in HPL. Shifted mass flow rate profile with  $\mu = 1.42$ ,  $\delta = 0.1$  and  $\phi = 0$ .

the cluster, being operated for about 4900 h during the year. It is most often switched ON/OFF every one, two or three hours, but longer operating periods of about 10 and 20 h are not uncommon. The low coverage of heating demand is the reason why higher CO<sub>2</sub> emissions are attained in the case of the entire system. In this case, all the tools available to enhance the system flexibility, i.e. HWTS and energy dissipation, are needed to increase the fraction of heating demand satisfied by the thermal network. The LTHE supplies about 73% of the LT cooling demand and is operated for about 6000 h a year on an hourly basis. It is most often switched ON/OFF every one, two, and three hours and common operating periods are shorter than 15 h. Similar considerations can be made for the HTHE, which supplies about 77% of the HT cooling demand.

The optimal behavior of the HPL geothermal field and cluster HWTS is illustrated in Fig. 9. As shown in Fig. 9-a, the temperature variation is less pronounced than for the HPL cluster when considered stand-alone. In both cases, such a temperature variation is significantly smaller than the exploitable range (from 8 °C to 22 °C, see Table 1) and than the temperature variation experienced by the geothermal fields under the current operation [42]. This suggests that a smaller geothermal storage capacity would be enough for the optimal operation of the Anergy Grid. Together with the evidence that lower CO<sub>2</sub> emissions can be achieved by coupling a demand cluster with a dedicated geothermal field (see comparison between Fig. 4-a and Fig. 8-a), this suggests an improved design of the Anergy Grid with more and smaller geothermal fields. Furthermore, two peaks are observed both in summer and winter, indicating a storage dynamic faster than seasonal. This is due to the necessity of meeting the variable energy demands of all clusters at the same time, and therefore to exploit the geothermal field through two storage cycles per year. Fig. 9-b shows the operation of the HWTS. This is mostly used to compensate the short-term mismatch between heat generation and demand, and it is mostly exploited in summer, hence allowing the heat pump to operate even in moments of low heat demand (low heat demands must be satisfied via HWTS since no energy dissipation occurs, i.e.  $\phi = 0$ ).

## 6. Conclusions

This paper investigates the optimal operation of MES deploying geothermal energy storage to cope with the seasonal variability of heating and cooling demands. The benefits of seasonal geothermal

storage are assessed and optimized with reference to a real-world system, namely the Anergy Grid installed at ETH Zurich, in Switzerland. In such a system, centralized heat and cold production based on fossil fuels is replaced by a dynamic underground thermal network connecting geothermal fields, which serve as energy source and storage, with demand clusters requiring thermal and cooling energy. The current system operation allows reducing the CO<sub>2</sub> emissions of the university campus by 72% with respect to the conventional system using centralized heating and cooling. The scope of this contribution is developing an optimization framework enabling further increase in energy efficiency, hence further emissions reduction.

To this end, we develop a novel optimization model that is able to address the complexity of the physical system, and that improves on the state-of-the-art by (i) accounting for the nonlinearities of the physical system, and (ii) capturing both the short- and long-term dynamics of energy conversion, storage and consumption. These features allow improving the current operation strategies and explaining the rationale behind the optimal system operation and design.

More specifically, the optimal system operation enables a CO<sub>2</sub> emissions reduction up to 87% with respect to the conventional system using centralized heating and cooling (though such a value comes at the cost of dissipating to the environment an amount of energy equal to the energy demand). This is achieved by operating the heat pumps and the heat exchangers on an hourly basis, i.e. by switching them ON/OFF every one, two and three hours. Furthermore, only deploying seasonal energy storage through geothermal fields enables a CO<sub>2</sub> emissions reduction up to 76% with respect to the conventional system. The full potential of the Anergy Grid is obtained by (i) selecting the optimal value of mass flow rate circulating through the network, which should vary with time and be high enough to satisfy the heating and cooling demands, but without exceeding either of the two, (ii) coupling the geothermal fields with HWTS, which allows maximizing the efficiency of energy storage from daily to seasonal cycles, (iii) releasing energy to the environment, which provides additional system flexibility when the heating and cooling demands are very different from each other. Finally, the optimal temperature evolution of the geothermal fields suggests that the design of the Anergy Grid could be improved by installing more and smaller geothermal fields, with each geothermal field having a dedicated demand cluster. Also, the positive effect of releasing energy to the environment points towards an optimal expansion of the Anergy Grid where heating and cooling demands are

better balanced, and the geothermal fields better exploited.

### CRedit authorship contribution statement

**Paolo Gabrielli:** Conceptualization, Software, Methodology, Visualization, Writing - original draft, Review & editing. **Alberto Acquilino:** Software, Formal analysis, Writing - original draft. **Silvia Siri:** Supervision, Review & editing. **Stefano Bracco:** Supervision, Review & editing. **Giovanni Sansavini:** Supervision, Visualization, Review & editing. **Marco Mazzotti:** Supervision, Visualization, Review & editing.

### Declaration of Competing Interest

The authors declare that they have no known competing financial interests or personal relationships that could have appeared to influence the work reported in this paper.

### Acknowledgments

The authors thank Raphael Wu (Reliability and Risk Engineering laboratory at ETH Zurich) for the very helpful and fruitful discussions during the analyses that led to the paper, Maria Yliruka (Department of Chemical Engineering at Imperial College London) for setting up the analysis of the geothermal fields, and Viola Becattini (Separation Processes Laboratory at ETH Zurich) for sharing helpful material concerning the analysis of the geothermal fields. Furthermore, the authors thank Dominik Brem, Wolfgang Seifert and Urs Hinnen (ETH Immobilien), as well as Marc Hausermann and Matthias Mast (Amstein-Walthert) for the very helpful discussions and insights on the operation of the Anergy Grid of ETH Zurich.

### Appendix A. Supplementary data

Supplementary data associated with this article can be found, in the online version, at <https://doi.org/10.1016/j.ecmx.2020.100052>.

### References

- [1] IPCC. Summary for Policymakers. In Global Warming of 1.5 C. An IPCC Special Report on the impacts of global warming of 1.5C above pre-industrial levels and related global greenhouse gas emission pathways, in the context of strengthening the global response to the threat of climate change. 2018. [Masson-Delmotte, V., P. Zhai, H.-O. Pörtner, D. Roberts, J. Skea, P.R. Shukla, A. Pirani, W. Moufouma-Okia, C. Péan, R. Pidcock, S. Connors, J.B.R. Matthews, Y. Chen, X. Zhou, M.I. Gomis, E. Lonnoy, T. Maycock, M. Tignor, and T. Waterfield (eds.)]. World Meteorological Organization, Geneva, Switzerland.
- [2] Dong Sig Chai, John Z. Wen, and Jatin Nathwani. Simulation of cogeneration within the concept of smart energy networks. *Energy Convers Manage* 75:2013;453–465.
- [3] van Leeuwen RP, de Wit JB, Smit GJM. Review of urban energy transition in the Netherlands and the role of smart energy management. *Energy Convers Manage Oct* 2017;150:941–8.
- [4] Delfino Federico, Bracco Stefano, Brignone Massimo, Rossi Mansueto, Robba Michela. Microgrid Design and Operation: Toward Smart Energy in Cities. Artech House; 2018.
- [5] Cao J, Crozier C, McCulloch M, Fan Z. Optimal design and operation of a low carbon community based multi-energy systems considering ev integration. *IEEE Trans Sustain Energy* 2019;10(3):1217–26.
- [6] Turk Ana, Qiuwei Wu, Zhang Menglin, Østergaard Jacob. Day-ahead stochastic scheduling of integrated multi-energy system for flexibility synergy and uncertainty balancing. *Energy* 2020;196:117130.
- [7] Mancarella Pierluigi. MES (multi-energy systems): an overview of concepts and evaluation models. *Energy* 2014;65:1–17.
- [8] Allegrini Jonas, Orehoung Kristina, Mavromatidis Georgios, Ruesch Florian, Dorer Viktor, Evins Ralph. A review of modelling approaches and tools for the simulation of district-scale energy systems. *Renew Sustain Energy Rev* 2015;52:1391–404.
- [9] David Grosspietsch, Marissa Saenger, Bastien Girod. Matching decentralized energy production and local consumption: a review of renewable energy systems with conversion and storage technologies. *Wiley Interdiscip Rev* 2019;e336.
- [10] Moser A, Muschick D, Gölls M, Nageler P, Schranzhofer H, Mach T, Ribas Tugores C, Leusbrock I, Stark S, Lackner F, Hofer A. A MILP-based modular energy management system for urban multi-energy systems: performance and sensitivity analysis. *Appl Energy* 2020;261:114342.
- [11] Di Somma Marialaura, Caliano Martina, Graditi Giorgio, Pinnarelli Anna, Menniti Daniele, Sorrentino Nicola, Barone Giuseppe. Designing of cost-effective and low-carbon multi-energy nanogrids for residential applications. *Inventions* 2020;5(1):7.
- [12] Liu Tianhao, Zhang Dongdong, Wang Shuyao, Thomas Wu. Standardized modelling and economic optimization of multi-carrier energy systems considering energy storage and demand response. *Energy Convers Manage Feb* 2019;182:126–42.
- [13] Comodi Gabriele, Bartolini Andrea, Carducci Francesco, Nagarajan Balamurugan, Romagnoli Alessandro. Achieving low carbon local energy communities in hot climates by exploiting networks synergies in multi energy systems. *Appl Energy* 2019;256:113901.
- [14] Hein Philipp, Zhu Ke, Bucher Anke, Kolditz Olaf, Pang Zhonghe, Shao Haibing. Quantification of exploitable shallow geothermal energy by using Borehole Heat Exchanger coupled Ground Source Heat Pump systems. *Energy Convers Manage Nov* 2016;127:80–9.
- [15] Guelpa Elisa, Bischi Aldo, Verda Vittorio, Chertkov Michael, Lund Henrik. Towards future infrastructures for sustainable multi-energy systems: a review. *Energy* 2019;184(C):2–21.
- [16] Cui Yuanlong, Zhu Jie, Twaha Ssennoga, Chu Junze, Bai Hongyu, Huang Kuo, Chen Xiangjie, Zoras Stamatis, Soleimani Zohreh. Techno-economic assessment of the horizontal geothermal heat pump systems: a comprehensive review. *Energy Convers Manage Jul* 2019;191:208–36.
- [17] Mancarella Pierluigi, Chicco Gianfranco, Capuder Tomislav. Arbitrage opportunities for distributed multi-energy systems in providing power system ancillary services. *Energy* 2018;161:381–95.
- [18] Arnaudo Monica, Topel Monika, Puerto Pablo, Widl Edmund, Laumert Björn. Heat demand peak shaving in urban integrated energy systems by demand side management – a techno-economic and environmental approach. *Energy* 2019;186:115887.
- [19] Kilkış Şiir, Krajačić Goran, Duić Neven, Rosen Marc A, Al-Nimr Moh'd Ahmad. Advancements in sustainable development of energy, water and environment systems. *Energy Convers Manage* 2018;176:164–83.
- [20] Aresti Lazaros, Christodoulides Paul, Florides Georgios. A review of the design aspects of ground heat exchangers. *Renew Sustain Energy Rev* 2018;92:757–73.
- [21] Bayer Peter, Attard Guillaume, Blum Philipp, Menberg Kathrin. The geothermal potential of cities. *Renew Sustain Energy Rev* 2019;106:17–30.
- [22] Self Stuart J, Reddy Bale V, Rosen Marc A. Geothermal heat pump systems: status review and comparison with other heating options. *Appl Energy* 2013;101:341–8.
- [23] Khalid F, Dincer I, Rosen MA. Development and analysis of sustainable energy systems for building HVAC applications. *Appl Therm Eng* 2015;87:389–401.
- [24] Sommerfeldt Nelson, Madani Hatef. In-depth techno-economic analysis of PV/Thermal plus ground source heat pump systems for multi-family houses in a heating dominated climate. *Solar Energy* 2019;190:44–62.
- [25] Alirahmi Seyed Mojtaba, Dabbagh Sajjad Rahmani, Ahmadi Pouria, Wongwises Somchai. Multi-objective design optimization of a multi-generation energy system based on geothermal and solar energy. *Energy Convers Manage* 2020;205:112426.
- [26] Zare V. A comparative thermodynamic analysis of two tri-generation systems utilizing low-grade geothermal energy. *Energy Convers Manage* 2016;118:264–74.
- [27] Pastor-Martinez E, Rubio-Maya C, Ambriz-Díaz VM, Belman-Flores JM, Pacheco-Ibarra JJ. Energetic and exergetic performance comparison of different poly-generation arrangements utilizing geothermal energy in cascade. *Energy Convers Manage Jul* 2018;168:252–69.
- [28] Sarah Van Erdeveweghe, Johan Van Bael, William D'haeseleer. *Energy Convers Manage*.
- [29] Gabrielli Paolo, Gazzani Matteo, Martelli Emanuele, Mazzotti Marco. Optimal design of multi-energy systems with seasonal storage. *Appl Energy* 2018;219:408–24.
- [30] Mazzoni Stefano, Ooi Sean, Nastasi Benedetto, Romagnoli Alessandro. Energy storage technologies as techno-economic parameters for master-planning and optimal dispatch in smart multi energy systems. *Appl Energy* 2019;254:113682.
- [31] Gabrielli Paolo, Poluzzi Alessandro, Kramer Gert Jan, Spiers Christopher, Mazzotti Marco, Gazzani Matteo. Seasonal energy storage for zero-emissions multi-energy systems via underground hydrogen storage. *Renew Sustain Energy Rev* 2020;121:109629.
- [32] Pinel Patrice, Cruickshank Cynthia A, Beausoleil-Morrison Ian, Wills Adam. A review of available methods for seasonal storage of solar thermal energy in residential applications. *Renew Sustain Energy Rev* 2011;15(7):3341–59.
- [33] Lott Melissa C, Kim Sang-Il. Technology roadmap: energy storage [Technical report]. International Energy Agency; 2014.
- [34] Gabrielli Paolo, Gazzani Matteo, Martelli Emanuele, Mazzotti Marco. A MILP model for the design of multi-energy systems with long-term energy storage. *Computer aided chemical engineering*. vol. 40 Amsterdam, Netherlands: Elsevier; 2017. p. 2437–42.
- [35] Hoffmann Maximilian, Kutzler Leander, Stolten Detlef, Robinius Martin. A review on time series aggregation methods for energy system models. *Energies* 2020;13(3):641.
- [36] Coelho António, Neyestani Nilufar, Soares Filipe, Lopes João Peças. Wind variability mitigation using multi-energy systems. *Int J Electr Power Energy Syst* 2020;118:105755.
- [37] Angrisani G, Diglio G, Sasso M, Calise F, Dentice d'Accadia M. Design of a novel geothermal heating and cooling system: energy and economic analysis. *Energy Convers Manage* 108:2016;144–159.
- [38] Schütz Thomas, Schraven Markus Hans, Fuchs Marcus, Remmen Peter, Müller Dirk. Comparison of clustering algorithms for the selection of typical demand days for energy system synthesis. *Renew Energy* 2018;129:570–82.
- [39] Gabrielli Paolo. Optimal design of multi-energy systems: From technology modeling to system optimization [Phd thesis]. ETH Zurich; 2019.
- [40] Rosen Marc A, Koohi-Fayegh Seama. Geothermal energy: sustainable heating and

- cooling using the ground. Chichester, UK: John Wiley & Sons Ltd; 2016.
- [41] ETH Zürich. The energy of tomorrow: Energy concept Anergy Grid ETH Hönggerberg; 2019. URL:<https://www.ethz.ch/content/dam/ethz/main/eth-zurich/nachhaltigkeit/infomaterial/ETHSustainability/181119&Anergienetz&A4&6s&E&RZ&Webversion&FINAL.pdf> [accessed 2019-11-04].
- [42] Amstein + Walther. Monitoring Energiekonzept Hönggerberg. Technical report, Zurich; 2018.
- [43] Soltani Reza, Dincer Ibrahim, Rosen Marc A. Thermodynamic analysis and performance assessment of an integrated heat pump system for district heating applications. *Appl Therm Eng* 2015;89:833–42.
- [44] Khalid Farrukh, Dincer Ibrahim, Rosen Marc A. Techno-economic assessment of a renewable energy based integrated multigeneration system for green buildings. *Appl Therm Eng* 2016;99:1286–94.
- [45] Miglani Somil, Orehounig Kristina, Carmeliet Jan. Integrating a thermal model of ground source heat pumps and solar regeneration within building energy system optimization. *Appl Energy* 2018;218:78–94.
- [46] Weber C, Shah N. Optimisation based design of a district energy system for an eco-town in the United Kingdom. *Energy* 2011;36(2):1292–308.
- [47] Mehleri ED, Sarimveis Haralambos, Markatos NC, Papageorgiou LG. Optimal design and operation of distributed energy systems: application to Greek residential sector. *Renew Energy* 51:2013;331–342.
- [48] Bracco Stefano, Dentici Gabriele, Siri Silvia. DESOD: a mathematical programming tool to optimally design a distributed energy system. *Energy* 2016;100:298–309.
- [49] Gabrielli Paolo, Gazzani Matteo, Mazzotti Marco. Electrochemical conversion technologies for optimal design of decentralized multi-energy systems: modeling framework and technology assessment. *Appl Energy* 2018;221:557–75.
- [50] Gabrielli Paolo, Fürer Florian, Mavromatidis Georgios, Mazzotti Marco. Robust and optimal design of multi-energy systems with seasonal storage through uncertainty analysis. *Appl Energy* 2019;238:1192–210.
- [51] Elsidio Cristina, Bischi Aldo, Silva Paolo, Martelli Emanuele. Two-stage MINLP algorithm for the optimal synthesis and design of networks of CHP units. *Energy* 2017;121:403–26.
- [52] Elsidio Cristina, Martelli Emanuele, Grossmann Ignacio E. A bilevel decomposition method for the simultaneous heat integration and synthesis of steam/organic Rankine cycles. *Comput Chem Eng* 2019;128:228–45.
- [53] Gray Harry B. Powering the planet with solar fuel. *Nat Chem* 2009;1(1). 7–7.
- [54] Carslaw HS, Jaeger JC. Conduction of heat in solids. Oxford Science Publications. Clarendon Press; 1986.
- [55] Per Eskilson. Thermal analysis of heat extraction boreholes [PhD thesis]. Lund University; 1987.
- [56] Zeng HY, Diao NR, Fang ZH. A finite line-source model for boreholes in geothermal heat exchangers. *Heat Transfer Asian Res* 2002;31(7):558–67.
- [57] Diao NR, Zeng HY, Fang ZH. Improvement in modeling of heat transfer in vertical ground heat exchangers. *HVAC&R Res* 2004;10(4):459–70.
- [58] Herbert Alan, Arthur Simon, Chillingworth Grace. Thermal modelling of large scale exploitation of ground source energy in urban aquifers as a resource management tool. *Appl Energy* 2013;109:94–103.
- [59] Belzile Patrick, Lamarche Louis, Rousse Daniel R. Semi-analytical model for geothermal borefields with independent inlet conditions. *Geothermics* 2016;60:144–55.
- [60] Lamarche Louis, Beauchamp Benoit. A new contribution to the finite line-source model for geothermal boreholes. *Energy Build* 2007;39(2):188–98.
- [61] Lamarche Louis, Beauchamp Benoit. New solutions for the short-time analysis of geothermal vertical boreholes. *Int J Heat Mass Transfer* 2007;50(7–8):1408–19.
- [62] Bernier Michel, Pinel Patrice, Labib Richard, Paillet Raphaël. A multiple load aggregation algorithm for annual hourly simulations of GCHP systems. *HVAC&R Res* 2004;10(4):471–87.
- [63] Yavuzturk C, Spitler JD. A short time step response factor model for vertical ground loop heat exchangers. In *ASHRAE Annual Meeting*, Seattle; 1999.
- [64] Miglani Somil, Orehounig Kristina, Carmeliet Jan. A methodology to calculate long-term shallow geothermal energy potential for an urban neighbourhood. *Energy Build* 2018;159:462–73.
- [65] Steen David, Stadler Michael, Cardoso Gonçalo, Groissböck Markus, DeForest Nicholas, Marnay Chris. Modeling of thermal storage systems in MILP distributed energy resource models. *Appl Energy* 2015;137:782–92.
- [66] Glover Fred. Improved linear integer programming formulations of nonlinear integer problems. *Manage Sci* 1975;22(4):455–60.
- [67] McCormick Garth P. Computability of global solutions to factorable nonconvex programs: Part I – convex underestimating problems. *Math Program* 1976;10(1):147–75.
- [68] Mitsos Alexander, Chachuat Benoit, Barton Paul I. McCormick-based relaxations of algorithms. *SIAM J Optim* 2009;20(2):573–601.
- [69] MathWorks. Matlab; 2018.
- [70] Löfberg J. Yalmip: a toolbox for modeling and optimization in matlab. In *Proceedings of the CACSD Conference*, Taipei, Taiwan; 2004.
- [71] IBM. ILOG CPLEX Optimization Studio; 2018.
- [72] ETH Zürich. The Anergy Grid of ETH Zurich; 2019. URL:<https://www.ethz.ch/en/the-eth-zurich/sustainability/campus/environment/energy/anergy-grid.html> [accessed: 2019-11-04].
- [73] Zurich ETH. Sustainability Report 2017/2018 [Technical report]. ETH Zurich; 2018.